

GainSight: Application-Guided Profiling for Composing Heterogeneous On-Chip Memories in AI Hardware Accelerators

Peijing Li
peli@stanford.edu
Stanford University
Stanford, CA, USA

Matthew Hung
mathu@stanford.edu
Stanford University
Stanford, CA, USA

Yiming Tan
yimingt@stanford.edu
Stanford University
Stanford, CA, USA

Konstantin Hoßfeld
hossfeld@stanford.edu
Stanford University
Stanford, CA, USA

Jake Cheng Jiajun
jiajunc@stanford.edu
Stanford University
Stanford, CA, USA

Shuhan Liu
shliu98@stanford.edu
Stanford University
Stanford, CA, USA

Lixian Yan
lxyn5869@stanford.edu
Stanford University
Stanford, CA, USA

Xinxin Wang
xxwang1@stanford.edu
Stanford University
Stanford, CA, USA

H.-S. Philip Wong
hspwong@stanford.edu
Stanford University
Stanford, CA, USA

Thierry Tambe
ttambe@stanford.edu
Stanford University
Stanford, CA, USA

ABSTRACT

As AI workloads drive soaring memory requirements, there is a need for higher-density on-chip memory for domain-specific accelerators that goes beyond what current SRAM technology can provide. We motivate that algorithms and application behavior should guide the composition of heterogeneous on-chip memories. However, there has been little work in factoring dynamic application profiles into such design decisions.

We present *GainSight*, a profiling framework that analyzes fine-grained memory access patterns and computes data lifetimes in domain-specific accelerators. By combining instrumentation and simulation across retargetable hardware backends, GainSight aligns heterogeneous memory designs with workload-specific traffic and lifetime metrics. Case studies on MLPerf Inference and PolyBench workloads using NVIDIA H100 GPUs and systolic arrays reveal key insights: (1) 40% of L1 and 18% of L2 GPU cache accesses, and 79% of systolic array scratchpad accesses across profiled workloads are short-lived and suitable for silicon-based gain cell RAM (Si-GCRAM); (2) Si-GCRAM reduces active energy by 11-28% compared to SRAM; (3) Up to 90% of GPU cache fetches are never reused, highlighting inefficiencies in terms of cache pollution. These insights that GainSight provides can be used to better understand the design spaces of both emerging on-chip memories and software algorithmic optimizations for the next generation of AI accelerators.

KEYWORDS

Heterogeneous on-chip memory, profiling, domain-specific accelerators, AI/ML workloads

1 INTRODUCTION

The surging size of AI models demands more on-chip memory to store intermediate results, as a means of optimizing spatial and temporal locality and improving energy efficiency [4, 15]. For a long time, microprocessors and accelerators have sought to keep up with this demand by steadily increasing on-chip static random access

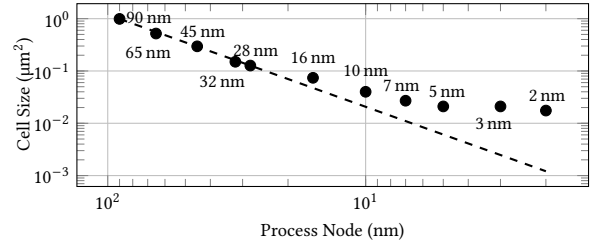


Figure 1: Scaling trend of 6T SRAM in recent process nodes, revealing a plateauing trajectory.

memory (SRAM) capacity with each new product generation. However, in recent years, SRAM scaling has slowed dramatically. Figure 1 shows the trend in standard 6-transistor SRAM cell sizes across advanced TSMC and Samsung process nodes [20, 55, 67, 69]. Since the 28 nm node, SRAM scaling has decelerated, and notably, from 5 nm to 3 nm, TSMC’s SRAM cell size has plateaued at $0.021 \mu\text{m}^2$ per cell. Although the transition to gate-all-around (GAA) transistors [69] at 2 nm offers certain transistor-level benefits, it falls far short of reviving SRAM scaling to earlier trajectories. Consequently, two perf/mm² challenges arise. First, increasing SRAM capacity leads to larger die sizes, and longer distances for data to travel, leading to higher latency, energy consumption and cost. Second, in case the die is already reticle-limited, adding more on-chip memory may come at the expense of logic area, forcing a potentially unwelcome trade-off between compute and memory. The slowdown in SRAM scaling has renewed interest in alternative on-chip memory devices that can provide higher density and improved fJ/bit efficiency [33, 41], leveraging their unique intrinsic properties that align better with application-specific memory traffic patterns.

Recent studies reveal that AI accelerator memory access patterns are split into short- and long-lived data [30]. In AI inference, short-lived data include frequently modified activations, while long-lived data include model weights, which are frequently read but rarely

Table 1: Comparison of on-chip memory devices

	SRAM	Long-term RAM	Short-term RAM
Structure	6T SRAM	MRAM, RRAM, FeRAM, etc.	2T/3T GCRAM, 1T1C eDRAM
Benefits	Long retention & balanced R/W perf.	Dense, 3D-stackable, long retention, low read energy	Dense, 3D-stackable, low leakage power
Drawbacks	Area scaling issues, high static power	Expensive writes, limited endurance	Short retention, expensive refreshes
Uses	Fast read and write caching	Rarely written, static data cache	Fast write-then-read ops. for dynamic data

modified [12, 66]. This contrast drives differentiated memory access requirements where short-term memory demands high-speed writes with superior endurance, while long-term memory prioritizes density and read efficiency. Therefore, a strategic opportunity arises to map short-lived data with the finite retention time of short-term memory while trading off write performance in long-term memory when it comes to long-lived data, enhancing both area and energy efficiency [33, 41]. Table 1 presents emerging memory technologies addressing these challenges, including SRAM and specialized long-term and short-term memories.

As candidates for long-term on-chip memory, RRAM and other non-volatile memories (NVM) offer high integration density and low read power but suffer from high write power and limited endurance, making them suitable primarily for static data storage [24]. These technologies have been successfully integrated into AI accelerators for neural network weights [10, 31, 64]. Concurrently, Gain Cell Random Access Memory (GCRAM) [7, 17, 34, 35] shows promise as a short-term memory solution, offering low access energy, improved density, and infinite endurance despite shorter retention times—making it ideal for intermediate activation results.

Navigating the varied design spaces and implementing these heterogeneous memory technologies in AI accelerators presents unique challenges. For instance, one key issue motivating this work concerns the effective use of GCRAM for short-term on-chip data memory. Given GCRAM’s retention times on the order of microseconds [7, 17, 72], precise data lifetime management is critical to minimizing refresh overheads and ensuring data integrity. It is therefore necessary to characterize the lifetime of data structures generated by accelerator workloads to determine whether they are short- or long-lived relative to GCRAM’s retention capabilities. Similar levels of insight are also needed to make informed design decisions about other forms of short- and long-term memories.

Thus to *gain* this *insight* into fine-grained memory access patterns for composing emerging on-chip memory devices, including but not limited to *gain* cell RAM, we introduce *GainSight*, an application profiler that analyzes dynamic workload behavior in AI hardware accelerators and reports, among other metrics, on-chip data lifetime statistics. Existing profilers are either too coarse-grained to capture detailed memory lifetime information on a per-byte access or per-instruction basis, or they are restricted to a single hardware platform. *GainSight* fills this gap with a profiling solution agnostic to specific workloads or algorithms, analyzing memory access patterns across diverse accelerator backends to provide memory device performance projections and heterogeneous memory design hints.

Table 2: Architectures leveraging emerging short or long-term on-chip memory devices

Name	Target Workload	Primary On-chip Memory Type
DaDianNao [11]	CNN inference	short-term 1T1C eDRAM
RANA [58]	CNN inference	short-term 1T1C eDRAM
CAMEL [72]	CNN/Transformer training	short-term 3T GCRAM
STT-AI Ultra [38]	CNN training/inference	long-term MRAM
CHIMERA [16]	CNN training	long-term RRAM

This “profile-guided architecture optimization” approach provides more accurate insights into on-chip memory composition by leveraging cycle-accurate execution behaviors rather than analytical heuristics or theoretical models.

The contributions of this work are as follows:

- A versatile profiler framework, **GainSight**, enabling analysis of **data lifetimes and fine-grained memory access patterns** to inform the area- and energy-efficient composition of heterogeneous and denser on-chip memories.
- **Retargetable hardware backends** for acquiring memory access patterns from a variety of accelerator workloads.
- An **analytical frontend** that utilizes profiling data to predictively evaluate design constraints and performance for emerging on-chip memory technologies.
- **Case studies** demonstrating *GainSight*’s efficacy in providing design insights for lifetime-aware hardware and software optimizations, such as refining write allocation cache policies and reducing cache pollution rates.

To facilitate further research in this domain, *GainSight*’s source code is available at <https://code.stanford.edu/tambe-lab/gainsight>, containing the submodules for the backend and frontend components, as well as a selection of workloads used in this work.

2 BACKGROUND AND RELATED WORK

There has been existing work on non-SRAM on-chip memory architectures in AI accelerators, as well as profiling tools that can analyze memory access patterns. However, we identified limitations in both of these research areas that we aim to address with *GainSight*: the former has yet to incorporate dynamic, runtime profiling data to inform their designs; and the latter has not been able to specifically provide fine-grained, per-variable analysis of memory access patterns in domain-specific accelerators.

2.1 Accelerators with Emerging Memories

The use of non-SRAM on-chip memory devices in AI accelerators has gained significant attention. Table 2 summarizes representative architectures from the past decade.

AI accelerator designs have navigated the limitations of their chosen on-chip memory devices through various strategies. DaDianNao masked eDRAM refresh latencies with a banked architecture, while RANA reduced refresh frequency by training CNNs to tolerate data loss. CAMEL minimized intermediate data lifetimes through training dataflow modifications and extended GCRAM retention with circuit-level techniques. STT-AI Ultra used a smaller RRAM buffer to mitigate frequent MRAM writes, and CHIMERA compressed gradient updates to reduce RRAM writes.

Table 3: Comparison of on-chip memory runtime profilers

Profiler	Target	Memory Granularity	Open-Source
MemSpy [37]	CPU	Cache Lines	✗
CacheGrind [54]	CPU	Cache Lines	✓
perf mem [32]	CPU	Cache Lines	✓
DProf [46]	CPU	Software Data Structures	✓
Nsight Compute [42]	GPU	Coarse-Grained, CUDA Kernel-level	✗
rocProfiler [2]	GPU	Coarse-Grained	✓
GMProf [73]	GPU	Accesses to Device/ Shared Memory	✓
GainSight (Ours)	Retargetable (GPU, Accelerators, etc.)	Cache Lines and byte-level accesses	✓

These architectures primarily targeted CNN workloads (e.g., ResNet [22]) and relied on predictable dataflows, such as convolutions and matrix multiplications, to estimate data lifetimes and access intensities. Such approaches failed to generalize to other machine learning components (e.g., normalization, pooling) or non-AI workloads like graph processing and scientific computing. GainSight seeks to augment and supercharge existing accelerator memory design efforts by providing a dynamic tool to explicitly evaluate metrics that are most relevant to integrating emerging memory technologies, such as data lifetimes and access patterns.

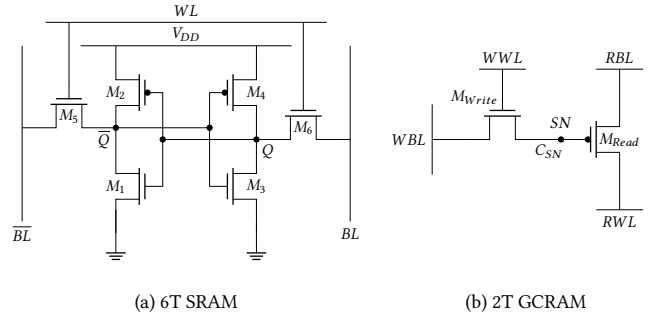
2.2 Hardware Profilers

Fine-grained memory access profiling is critical for aligning on-chip memory behavior with device properties of emerging memory technologies. Table 3 compares representative system and memory-level profilers with GainSight.

Extensive research has explored memory access profiling in CPUs. Modern CPUs feature performance counters that sample memory events at address-level granularity, such as Linux perf mem [32]. MemSpy [37] uses full-system simulation to track fine-grained memory accesses at specific addresses and cache behavior. Cachegrind [40, 54] offers similar profiling capabilities but lacks advanced modeling of prefetching and out-of-order execution. DProf [46] correlates sampled cache misses with program structures, identifying inefficiencies in data layout and cache utilization.

In contrast, domain-specific architectures such as GPUs and other emerging accelerators lack comparable fine-grained profiling capabilities. Existing GPU profilers, such as NVIDIA’s Nsight Compute [42], CUPTI [43] and AMD’s rocProfiler [2], provide high-level insights at kernel granularity but fail to characterize individual memory access behaviors. GMProf [73] leveraged GPU hardware features and static analysis to achieve finer granularity, but its abstract memory constructs do not directly map to physical on-chip memory arrays. In the meantime, profiling capabilities for non-GPU AI/ML accelerators remain underdeveloped.

Existing profilers are constrained by limited architectural support or insufficient granularity, lacking the resolution to capture memory lifetime information at per-byte or per-instruction levels. Additionally, proprietary tools like MemSpy and NVIDIA Nsight Compute are not readily extensible. GainSight addresses these gaps

**Figure 2: Comparison of 6T SRAM and 2T GCRAM circuits.**

by offering an open-source, extensible framework designed to support diverse accelerator architectures and workloads, while enabling research in fine-grained memory profiling.

2.3 GCRAM as Short-term Memory

One of the memory devices that the current implementation of GainSight focuses on is gain cell RAM (GCRAM) as a logic-compatible alternative to SRAM for storing short-lived data [7]. GCRAM designs vary in transistor counts (2T, 3T) and materials (silicon or oxide semiconductors), but they generally offer higher density and lower leakage power than SRAM, with trade-offs in performance and integration [34]. A comparison between the circuitry of 6T SRAM and 2T GCRAM is shown in Figure 2.

Silicon-based GCRAM (Si-GCRAM) designs [7, 17, 39] uses two or three transistors (2T or 3T) fabricated from fully silicon logic transistors. They typically achieve high read performance, but suffer from comparatively short μ s-scale retention times independent of write frequency.

Recent efforts explore non-silicon materials, such as indium tin oxide (ITO), for 2T GCRAM devices [9]. ITO transistors, fabricated at back-end-of-line (BEOL) levels, enable 3D stacking for higher density. Fully oxide designs use ITO for both read and write transistors, while hybrid designs combine silicon for the pMOS read transistor and oxide materials for nMOS the write transistor [36, 56]. These GCRAM devices achieve significantly longer retention times, up to seconds [36], but retention decreases with higher write frequencies [34], motivating profiling strategies to optimize hardware and software trade-offs.

3 DEFINING DATA LIFETIMES

We introduce the definition of data lifetimes and discuss specifications for measuring them through profiling, motivated by the need to evaluate the feasibility of composing retention-constrained emerging memory technologies—such as short-term GCRAM or 1T1C eDRAM—into on-chip memory for specific workloads. Understanding the lifetime of data structures is essential to determine whether these devices’ retention times are adequate for the workload’s requirements.

3.1 Basic Definition

The intuitive understanding of lifetimes of data values stored on on-chip memory devices is as follows:

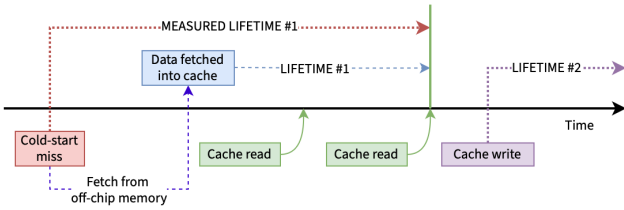


Figure 3: Ideal and Measured lifetime definitions for repeated accesses to a data value at a single memory address.

Definition 3.1. One **lifetime** of a value with a given address in the on-chip memory is defined as the time between the **first write** of that value to that address and the **last read** of that value from that address before it is overwritten or invalidated.

Definition 3.1 is illustrated in Figure 3 as the interval between the first write to a memory address and the last read before the next write. Several considerations extend Definition 3.1:

- (1) There is an etymological distinction between “reads/writes” and “loads/stores”: processing elements (PEs) use load/store instructions to access data in the memory hierarchy, which may result in the memory being read or written to.
- (2) Multiple values may be written to the same subpartition with the same address, creating multiple data lifetimes.
- (3) Lifetimes are initiated by the first write in two ways: directly from the PE via a store instruction, or fetched from off-chip memory to the on-chip memory.
- (4) The end of a lifetime can be identified in the following ways: (i) a subsequent store instruction overwrites the value, (ii) a subsequent fetch from off-chip memory overwrites the value, or (iii) program termination invalidates the value.
- (5) Between the first write and last read, multiple reads may occur, and the value must remain uncorrupted. This requires either that the memory device’s retention time exceeds the data lifetime or that the value is refreshed before the retention period lapses.

3.2 Scratchpad Memories

Scratchpad memories are prevalent in domain-specific accelerator architectures. Unlike traditional caches, they typically lack standard allocation, eviction, or coherence protocols, requiring explicit management through instructions executed by PEs. By monitoring these load/store instructions and management operations in profiling logs, we can adapt Definition 3.1 to measure data lifetimes in scratchpad memories.

Definition 3.2. One **lifetime** of a value in a **scratchpad memory** can be measured as the time between either a **store instruction** or a **fetch request** and the **last read** of that value before it is overwritten or invalidated.

An important caveat arises regarding the fetch operation. There is a delay between the issuance of a fetch request and the data being written to the scratchpad memory. The latter presents a more precise starting point for the lifetime of the data, as shown by “LIFETIME #1” in Figure 3. However, pinpointing this moment can be challenging, as it depends on the specific memory architecture

and the timing of data transfers. In practice, GainSight uses the issuance of the fetch request as a proxy for the start of the lifetime, as shown by the “MEASURED LIFETIME #1” in Figure 3—since this event is more readily observable across target architectures. Consequently, the lifetimes measured by GainSight may serve as conservative estimates of the actual data lifetime requirements.

3.3 Data Caches

Traditional data caches, as seen in CPUs and GPUs, are typically managed by hardware and are not explicitly controlled by software in terms of allocation and eviction – thus these key operations are not often recorded in the profiling logs. When adapting Definition 3.2 to data caches, we can utilize the concepts of cache hits and misses of fetch operations to delineate data lifetimes.

Definition 3.3. One **lifetime** of a value in a **data cache line** can be measured as the time between either a **store instruction** or a **cache miss** to that cache line and the **last cache hit on a read instruction** of from that cache line before either the next store instruction or a cache miss to that cache line.

In other words, the start of data lifetimes on fetch operations can be represented by cache misses, and the end of data lifetimes before the data is evicted from the cache can be represented by the last hit before the next miss.

3.3.1 Cache Write Allocation Policies. Cache allocation policies determine how cache lines are allocated for cache misses on write operations and how lifetimes are initiated. Under allocate-on-write, a store instruction to data not in cache fetches the data from the next level of memory and allocates a new cache line for it, initiating a new lifetime. Thus, any cache miss initiates a data lifetime. Conversely, no-allocate-on-write policy does not allocate cache blocks for write misses, initiating lifetimes only on read misses.

These approaches reflect trade-offs in managing data locality. Allocate-on-write may better exploit temporal locality but can cause cache pollution by allocating cache lines for one-time writes that are never reused. No-allocate-on-write reduces unnecessary allocations but may increase cache misses for workloads with overlapping read-write patterns. Section 7.1.4 explores these trade-offs in depth, with particular attention on their data lifetime implications.

3.4 Data Lifetime vs. Memory Retention

Measuring data lifetimes as defined previously is crucial for evaluating the suitability of retention-constrained memory devices and determining appropriate refresh requirements. These measurements enable informed design decisions regarding memory device selection and allocation of data structures based on their runtime behavior. As an illustrative example, Figure 4 compares the memory retention times and data lifetimes from various subroutines of the Llama 3.2 vision-language model (11B parameters) [18] running on an NVIDIA H100 backend. A few key observations are as follows:

- (1) Si-GCRAM retention time remains constant regardless of write frequency, while Hybrid-GCRAM’s initially higher retention time starts decreasing at higher write frequencies, as discussed in Section 2.3.
- (2) GEMM operations exhibit the shortest data lifetime – below Si-GCRAM’s retention time – enabling refresh-free storage

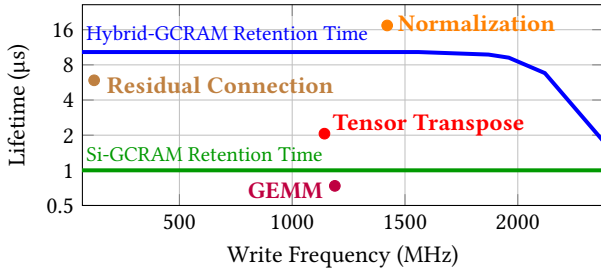


Figure 4: Comparison of write frequencies and data lifetimes for selected operations in the Llama-3.2-11b vision model [18] executed on NVIDIA H100 backend, against the retention times of Si-GCRAM and Hybrid-GCRAM [34].

of intermediate values in the more area-efficient Si-GCRAM within a heterogeneous memory system.

- (3) Tensor transpose and residual connection operations have data lifetimes exceeding Si-GCRAM’s retention time but remaining below that of Hybrid-GCRAM, making Hybrid-GCRAM optimal for these operations.
- (4) Normalization operations require longer retention times than both GCRAM variants provide. This therefore necessitates quantitative analysis to determine the energy costs of refresh and to compare the overall area and energy efficiencies against those of SRAM.

This relationship between data lifetimes and device retention capabilities forms the conceptual foundation for evaluating refresh-constrained memory devices and their workload suitability, underpinning the entire GainSight profiler framework.

4 GAINSIGHT ORGANIZATION

GainSight is designed as a comprehensive framework for analyzing on-chip memory behavior, addressing the question: “For a given workload or a set of workloads executed on a target hardware accelerator backend, what are the tangible benefits of replacing on-chip SRAM with emerging memory device arrays in terms of area and energy consumption?”

To answer this, GainSight performs the following key tasks:

- (1) Captures fine-grained traces or logs of on-chip memory access behavior for arbitrary workloads executed on a target hardware backend.
- (2) Extracts key statistics, e.g., data lifetimes, read/write frequencies, and memory capacity utilization, from the logs.
- (3) Correlates these statistics with the attributes of various memory technologies to project key performance indicators (KPIs) for these memory devices under workload execution.
- (4) Visualizes the projected KPIs through an interactive interface, informing decision-making for memory array design.

To meet these requirements, GainSight comprises two primary components: a set of retargetable hardware backends and a flexible analytical frontend, as illustrated in Figure 5. The backend is responsible for executing workloads on specific hardware architectures and generating fine-grained, cycle-accurate memory access traces. The frontend processes these traces to extract key statistics, correlates them with memory device attributes, and projects

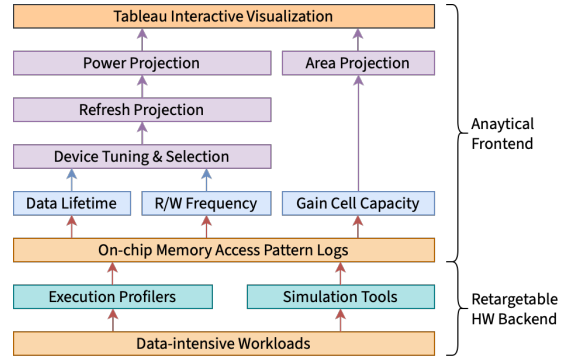


Figure 5: GainSight tool organization, comprising of retargetable hardware backends and a flexible analytical frontend. The input, output, and intermediate files are colored in orange, backend components are colored in teal, frontend log parsing components are colored in blue, and frontend projection and analysis components are colored in purple.

the devices’ performance metrics. It also provides Tableau-based interactive visualization tools to facilitate design space exploration.

The following sections detail the design and implementation of the backend and frontend components, highlighting their roles in achieving GainSight’s objectives.

5 RETARGETABLE HARDWARE BACKEND

The memory access patterns and data lifetimes for even similar workloads may vary significantly across different hardware architectures. The organization of on-chip memory also differs substantially between architectures. Therefore, we designed GainSight to support multiple hardware backends, making it uniquely flexible and extensible.

The primary function of the GainSight backend is to provide fine-grained memory access traces that can be used to most accurately evaluate how well a given workload fits with different on-chip memory architectures. Thus each hardware backend must produce detailed, fine-grained logs or traces documenting how workloads interact with on-chip memories, including cycle-accurate records of memory accesses with address, type (read/write), timing, size, and hit/miss status.

Given this granularity requirement, state-of-the-art runtime profilers for physical hardware tend to lack the detail needed to produce the memory access traces required for this study, as mentioned in Section 2.2. To address this limitation, we adopted simulation-based approaches, modifying existing simulators to generate the required traces. Our implementation includes backends for simulating NVIDIA GPUs and systolic array-based accelerators.

5.1 Backend 1: Simulating NVIDIA GPUs

NVIDIA GPUs, built on a single instruction, multiple data (SIMD) architecture, have become a leading standard for accelerating deep learning workloads, with application potential expanding as rapidly as their computational and memory demands. Figure 6 details our simulation-based backend implementation for these devices.

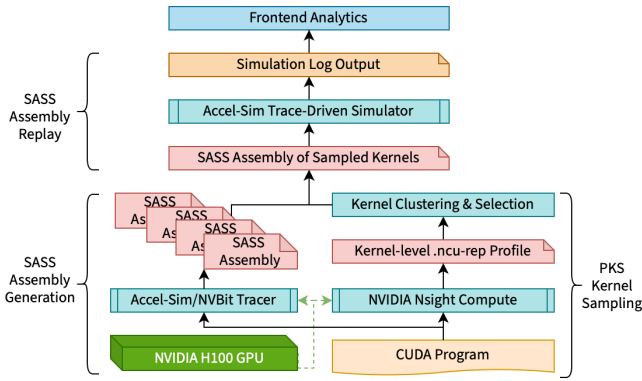


Figure 6: NVIDIA GPU simulation-based backend organization. The color scheme is the same as Figure 5; in addition, the physical GPU hardware is colored in dark green, and the intermediate files specific to this backend are colored in red.

This backend comprises three main components: an NVBit [61]-based tracing utility capturing SASS assembly code for each kernel, a kernel clustering and sampling utility using coarse-grained profiling information to select a subset of the kernels to simulate, and a cycle-accurate simulator that simulates the selected kernels and generates memory access traces. The tracer and simulator are adapted from Accel-Sim [29], while the kernel clustering utility builds on Principal Kernel Analysis (PKA) [5]. This enables cycle-accurate simulations for arbitrary CUDA programs.

5.1.1 Adapting Accel-Sim. The Accel-Sim simulator is a cycle-accurate simulator for NVIDIA GPUs that can simulate the execution of CUDA kernels on a GPU architecture [29]. In this work, we specifically used version 1.3.0 of the Accel-Sim simulator as a backend representing the NVIDIA H100 GPU. Accel-Sim’s trace-driven execution capability allows running SASS assembly code, i.e., the proprietary NVIDIA ISA specific to each GPU microarchitecture, on a cycle-accurate GPU model, simulating execution across streaming multiprocessors (SMs) and various levels of the memory hierarchy, including L1 and L2 caches, HBM memory, and their interconnects.

As shown in Figure 6, we first execute workloads on physical GPU hardware, using NVBit to capture SASS assembly code for each kernel. These traces are then fed into GPGPU-Sim v4.2.1 [6, 29] to simulate and step through program execution and collect memory access traces at each individual cycle and instruction.

We modified Accel-Sim by inserting logging calls at SM-L1 and L2-HBM interfaces to record address, access type, timing, and hit/miss status of each cache operation. While NVIDIA GPUs contain multiple on-chip memory components, we focus on L1 and L2 caches, which are most relevant for AI/ML workloads and present the greatest opportunity for energy and area optimization.

5.1.2 Ablation Studies on Write Allocation. Accel-Sim and GPGPU-Sim allow arbitrary configuration of on-chip memory subpartitions, including cache sizes, block sizes, associativity, and replacement policies. Given the impact of cache write allocation policies on data lifetime measurement, we compared statistics by configuring L1

Table 4: Key runtime metrics of Principal Kernel Selection [5] applied to selected AI workloads running on the Accel-Sim [29] backend.

Workload	% Sampled	Speedup	Avg Lifetime MAE (μ s)	Write Freq MAE (MHz)	Area MAE (mm^2)	Energy MAE (kJ)
bert-base-uncased	8.37%	10.89	0.36	11.59	0.00	1.09
llama-3-8b	0.15%	412.76	3.76	21.39	0.91	3.65
resnet-50	10.31%	60.97	3.73	10.09	0.00	1.99

and L2 data caches as either write-allocate or no-write-allocate, as expanded in Section 7.1.4.

5.1.3 Simulator Performance and Program Sampling. Cycle-accurate simulation in Accel-Sim can be 6-7 orders of magnitude slower than native GPU execution, potentially requiring days to months for large language model inference tasks [60]. However, deep learning workloads are highly repetitive, with similar layer structures repeated throughout models [22, 59] or the same layer executed multiple times across different input subsets [8, 23]. Restuccia and Biondi [51] empirically confirmed minimal variation in memory access patterns between AI model layers, enabling workload sampling while maintaining statistical accuracy. Our sampling methodology adapts the PKA algorithm [5] to select representative kernels. This process (Figure 6, bottom right) involves:

- (1) Running workloads on H100 GPUs using NVIDIA Nsight Compute to gather offline, coarse-grained profiling data on each kernel’s general characteristics, such as numbers of reads or writes, cache hits or misses, and execution time.
- (2) Applying Principal Component Analysis (PCA) to reduce dimensionality of per-kernel profiling results.
- (3) Using K-means clustering to group kernels based on PCA results, determining cluster count by measuring how each number of clusters affects the prediction accuracy for L2 cache line writes.
- (4) Selecting the kernel closest to the cluster centroid for each cluster, and simulating only these representative kernels.

As shown in Table 4, sampling reduces the number of simulated kernels from potentially thousands to fewer than 20, achieving over 100 \times speedup and making it feasible to evaluate models from the MLPerf Inference benchmark suite [50] that would otherwise be impractical to simulate. Despite this optimization, the sampling algorithm preserves reasonable accuracy in key metrics such as data lifetimes and write frequencies, which are critical for evaluating memory devices and projecting memory array area and energy consumption, as discussed in more detail in Section 6.

Our sampling approach is extensible to other backends, enabling acceleration of all simulation-based evaluations.

5.2 Backend 2: Simulating Systolic Arrays

For systolic array-based accelerators, we extend the open-source SCALE-Sim [53], a Python-based simulator for convolution or GEMM-based DNN networks. This model utilizes three peripheral SRAM buffers: input (*ifmap*), weight (*filter*), and output (*ofmap*). SCALE-Sim provides a range of features that we leverage for our backend: (1) cycle-accurate simulations; (2) configurable sizes for the on-chip *ifmap*, *ofmap*, and *filter* buffers; (3) configurable dataflow

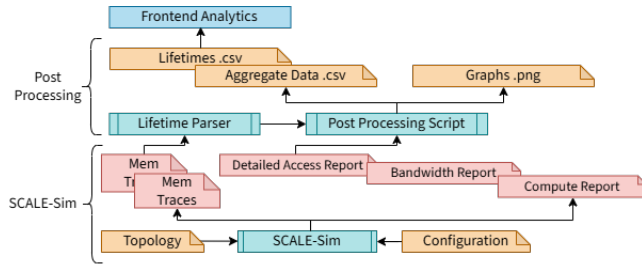


Figure 7: Systolic array backend organization.

and processing element (PE) array dimensions; and (4) built-in memory access trace generation.

The memory traces group data by buffer banks and datatypes as well as by memory levels. For ifmap and weight buffers, we interpret DRAM accesses as *memory writes* and SRAM accesses as *memory reads*, with the opposite for ofmap data where PE outputs are written to SRAM before transfer to DRAM.

Workload simulation requires encoding the network topology into a YAML file in either CNN format (with filter dimensions, channels, strides) or transformer format (with GEMM parameters M, N, K). From these memory traces, we extract data lifetimes following Definition 3.2, calculating them by identifying writes and subsequent latest reads before new writes. Initial data lifetime results are reported in terms of cycles; while SCALE-Sim does not explicitly define a clock frequency, we use an assumed frequency of 1 GHz for our analysis. Using SCALE-Sim data and Python’s pandas library [44, 65], we can extract aggregate statistics like unique address accesses and data lifetimes (Figure 7) from the raw memory traces.

5.3 Bring Your Own Hardware Backend

GainSight is not confined to the two backends discussed above. The profiler’s frontend, as detailed in the next section, is designed to process memory access traces or logs generated by any hardware backend, provided they adhere to a standard including detailed timestamps, address ranges, read/write types, and hit/miss status for each memory hierarchy access. Consequently, hardware simulators or physical devices capable of generating fine-grained memory access traces can be seamlessly integrated as alternative backends, leveraging the existing GainSight analytical frontend.

Nonetheless, it is crucial to acknowledge the architectural heterogeneity among potential hardware backends. These differences extend beyond the PEs themselves – such as the contrasting dataflow paradigms of systolic arrays and SIMD architectures like GPUs – to the organization of on-chip memory. For instance, NVIDIA GPUs feature a hierarchical memory structure comprising L1 and L2 caches, alongside auxiliary modules like instruction and shader caches, which GainSight does not explicitly profile. In contrast, systolic arrays employ SRAM scratchpads dedicated to model weights and input/output feature maps.

To address these architectural disparities, GainSight introduces the generic concept of memory “subpartitions.” Subpartitions abstractly represent distinct memory components, such as cache levels in GPUs or scratchpad buffers in systolic arrays. The frontend treats

each subpartition as an independent entity when calculating metrics such as data lifetimes, read/write frequencies, chip area, active energy consumption, and other performance statistics.

6 ANALYTICAL FRONTEND

The profiler frontend processes memory access traces from hardware backends to compute key on-chip memory statistics, including data lifetimes, read/write frequencies, and capacity utilization. These metrics are correlated with on-chip memory device characteristics to produce JSON reports and Tableau-based visualizations. Designed for flexibility using unified Python scripts, the frontend accommodates diverse backends and memory types. Subsequent sections detail its implementation.

6.1 On-chip Memory Statistics

Key considerations in heterogeneous on-chip memory design include data lifetimes, read/write frequencies, and capacity utilization. These metrics are derived from raw memory access traces as described in Section 5. Data lifetimes are computed as outlined in Section 3. Read/write frequencies are calculated by counting clock cycles with memory operations and normalizing by the total clock cycles in the workload. Capacity utilization is determined by counting unique memory addresses accessed, scaled by the memory block size that each address maps to. This metric quantifies actual workload memory usage, which may be less than the total available capacity of an on-chip memory array.

6.2 Memory Device Model Correlation

After computing memory statistics for each subdivision, these data are correlated with the performance of the corresponding memory device. The current GainSight implementation evaluates short-term memory devices, namely GCRAM and SRAM. Available devices include 6T SRAM, 2T silicon gain cell RAM (Si-GCRAM), and 2T OS-Si hybrid gain cell RAM (Hybrid-GCRAM), modeled using the TSMC N5 process node. For each device, we could determine its retention times (and its relation to write frequency), bit cell area, and average read/write energy per bit. SRAM statistics were derived from TSMC specifications in [69, 70]. Si-GCRAM statistics were based on Giterman et al. [17] and Pentecost et al. [45]’s fabricated arrays and then scaled to the N5 process nodes. Hybrid-GCRAM statistics were obtained from the GEMTOO array-level simulations [7] of 256x256 GCRAM arrays by Liu, et al. [34, 35], and then scaled to the TSMC N5 process node.

As shown in Figure 5, the GainSight frontend uses the maximum write frequency encountered in the dynamic profile of a workload to compute memory device retention times. By aligning these with observed data lifetimes, we estimate the refresh cycle requirements for each memory device. For example, a data structure with a 10 ns lifetime requires two refreshes for a memory device with a 4 ns retention time. The refresh requirement is computed as:

$$R = \sum_k \left\lceil \frac{T_k}{t_r} \right\rceil \cdot B_k, \quad (1)$$

where T_k , t_r , and B_k represent the data lifetime, device retention time, and bit-width per data value, respectively. Each refresh is approximated as a read followed by a write. Given the number

of refreshes and the measured number of reads and writes from the backend, the total active energy that a retention-constrained memory array consumes over the execution of the target workload can be calculated as:

$$E_{active} = E_r \cdot (N_r + R) + E_w \cdot (N_w + R), \quad (2)$$

where E_r , E_w , N_r , and N_w denote the read/write energies and read/write counts, respectively.

By enumerating the unique memory address ranges accessed, it is possible to quantify the capacity requirement for each level or subdivision of the on-chip memory hierarchy. The capacity requirements can then be used to estimate the physical area of an on-chip memory device as follows:

$$A = A_{cell} \cdot B_{addr} \cdot N_{addr}, \quad (3)$$

where A_{cell} denotes the area of a single bit cell, B_{addr} corresponds to the number of bits per address, and N_{addr} indicates the total number of unique memory addresses accessed.

The frontend generates a JSON report summarizing device retention times, refresh requirements, active energy consumption, and area requirements. These results are visualized in the next stage.

6.3 Visualization

To enable comprehensive data lifetime analysis across diverse architectural configurations and workloads, we developed a visualization framework using Tableau [52]. This framework uses a suite of interactive graphical representations to present profiling results and elucidate relationships between key metrics generated by both the frontend and backend components.

Our Tableau visualization interface incorporates various data representations, including lifetime distribution histograms and comparative scatter plots illustrating projected memory array characteristics, including area utilization and energy consumption across different memory technologies.

A notable feature of our Tableau-based interface is its advanced interactive filtering capability, which allows users to dynamically segment and compare memory access patterns via interactive UI elements. Histograms and scatter plots in this visualization framework also enable the inspection of individual data points, each representing a specific workload kernel. The tooltips on the plots provide additional information such as specific workload, kernel, subdivision, and the corresponding values of data lifetimes, read/write frequencies, or capacity utilization.

Our Tableau-based GainSight visualization framework is publicly accessible at <https://gainsight.stanford.edu>. This open access aims to support further exploration of our findings and to advance research on integrating emerging memory technologies into next-generation accelerator architectures.

7 CASE STUDY AND EXPERIMENTS

To demonstrate GainSight’s capabilities, we conducted two case studies utilizing the NVIDIA H100 GPU and systolic array backends implemented in the profiler.

We executed a set of workloads from MLPerf Inference benchmark (v5.0) suite [50] and PolyBench [19, 47] on both backends, analyzing the memory access patterns, data lifetimes, and the projected performance of the GCRAM variants, as well as SRAM. PolyBench’s

Table 5: List of workloads executed in GPU case study.

Name	Test Suite	Description
2dconvolution	PolyBench	2D Convolution
3dconvolution	PolyBench	3D Convolution
llama-3.2-1b	ML Inference	Meta’s text-based LLM with 1 billion parameters [57]
llama-3-8b	ML Inference	Meta’s text-based LLM with 8 billion parameters [57]
llama-3.2-11b-vision	ML Inference	Meta’s LLM with integrated a vision adapter for image recognition, total of 11 billion parameters [57]
resnet-18	ML Inference	CNN for image recognition with 18 layers [22]
resnet-50	ML Inference	CNN for image recognition with 50 layers [22]
bert-uncased-110m	ML Inference	“Bidirectional Encoder Representation for Transformers,” [13] text-based LLM with 110 million parameters
gpt-j-6b	ML Inference	GPT-like text-based LLM with 6 billion parameters [62, 63] implemented on the JAX interface
stable-diffusion-3.5b	ML Inference	Text-to-image transformer model with 3.5 billion parameters [14]

CUDA implementation involves basic linear and matrix algebra operations on randomized inputs of predetermined sizes. MLPerf Inference includes pretrained machine learning models representing state-of-the-art AI development. These models represent two common AI/ML inference tasks: text generation via transformers and image recognition/generation via CNNs or transformers.

For the GPU backend, we performed an ablation study on the impact of write allocation policies and cache pollution. For the systolic array backend, we investigated the influence of different dataflows on memory access patterns and data lifetimes. In the analytical frontend, we specifically focused on how suitable each workload is for a hypothetical short-term on-chip GCRAM array. These case studies illustrate the workflow of *profile-guided architecture optimization*, showcasing GainSight’s insights into application runtime behavior and memory device characteristics.

7.1 Profiling GPU Workloads

The first case study involves the Accel-Sim -based backend of the NVIDIA H100 GPU, as described in Section 5.1. GainSight was employed to analyze memory access patterns and project GCRAM device KPIs across workloads derived from the PolyBench and MLPerf Inference benchmark suites. The configurability of the backend also enables us to evaluate the impact of cache write allocation policies on data lifetime and investigate cache pollution.

7.1.1 Workloads. The workloads used in this study are listed in Table 5. We selected these workloads to cover prominent use cases of AI inference acceleration in edge and cloud computing applications so as to quantify the potential area and energy benefits from adopting retention-constrained memory devices.

For transformer-based workloads, we configured inference tasks with a 7-word input prompt and a fixed token generation length of 20. For vision workloads, we used a 224×224 pixel input image size and a batch size of 1. The vision transformer was prompted to “summarize the image” with a maximum token generation of 20.

Additional workloads from PolyBench and MLPerf Inference were executed but are omitted here for brevity. Data and visualizations for these workloads are available via the GainSight Tableau-driven interactive interface described in Section 6.3 as part of this paper’s artifacts.

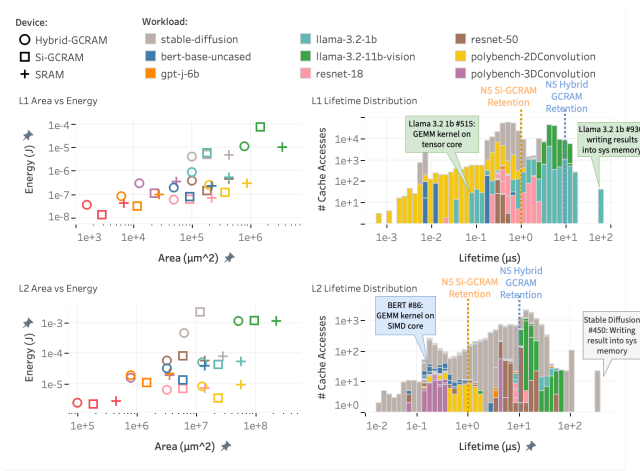


Figure 8: GainSight’s Tableau-based visualization of (left) the area and energy consumption for the L1 (top) and L2 (bottom) caches, and (right) their lifetime distributions compared against simulated 5nm Si-GCRAM and Hybrid-GCRAM retention times. [34].

7.1.2 Lifetime Observations. Figure 8 illustrates lifetime and on-chip GCRAM area/energy projections for L1 and L2 caches in the simulated H100 GPU for a subset of representative workloads.

The scatter plots on the left illustrate different projected area and energy requirements for L1/L2 caches using SRAM, Si-GCRAM, or Hybrid-GCRAM, reflecting workload-dependent demands and cache access patterns. The histograms on the right show the data lifetime distributions for the L1 and L2 caches, enabling a more direct comparison with the retention times of short-term memory devices.

These visualizations, explorable via GainSight’s Tableau interface with filtering capabilities, offer insights into memory characteristics across diverse workloads. The Tableau-based interface also allows users to filter the plotted data by workload, cache type, and memory device, enabling a more tailored analysis of the data lifetimes and their implications for memory device selection.

A key observation is the distinct bifurcation of data lifetimes. A significant fraction exhibits lifetimes short enough for refresh-free storage in short-term memories; for instance, approximately 39.5% of all L1 and 18.4% of all L2 accesses have lifetimes under the 1 μ s retention of 5nm Si-GCRAM [34]. Conversely, another substantial portion of data values on the two cache levels persists much longer (up to 70 μ s or more), incurring significant refresh overheads if placed in short-term devices and underscoring the need for heterogeneous memory architectures with varying retention times [30].

Kernel-level analysis further reveals that short-lived data often originate from linear algebra operations (e.g., GEMM kernel ID 515 in llama-3.2-1b), while long-lived data frequently arise during data transfers between system memory and GPU HBM (e.g., kernel ID 450 in stable diffusion). These kernel-level observations highlight potential optimization targets for different subroutines within a workload.

Table 6: Active energy ratios of Si-GCRAM (“Si-Si”) and Hybrid-GCRAM (“Hybrid”) to SRAM for L1 and L2 caches.

Workload	L1 Si-Si	L1 Hybrid	L2 Si-Si	L2 Hybrid
bert-base-uncased	33.53%	84.81%	35.37%	85.00%
gpt-j-6b	33.23%	84.81%	49.71%	87.49%
llama-3-8b	33.23%	84.81%	82.06%	84.85%
llama-3.2-11b-vision	681.61%	103.90%	98.41%	96.65%
llama-3.2-1b	1179.41%	172.35%	77.35%	93.73%
polybench-2DConvolution	41.74%	84.81%	35.96%	84.81%
polybench-3DConvolution	33.23%	84.81%	57.38%	84.81%
resnet-18	90.73%	84.81%	96.16%	88.73%
resnet-50	33.23%	84.81%	145.37%	100.77%
stable-diffusion	104.96%	84.81%	2817.53%	559.43%

Takeaway 7.1. Data lifetimes exhibit a clear bifurcation between short and long-lived categories, with long-lived lifetimes often concentrated in specific kernels, such as pooling or activation functions.

7.1.3 Active Energy Comparisons. An important observation pertains to the active energy consumption of Si-GCRAM and Hybrid-GCRAM, including energy costs associated with all reads, writes, and refreshes. This metric has received limited attention in the literature, where prior studies have predominantly focused on evaluating static and parasitic energy consumption.

For each workload, we quantified the active energy consumption of L1 and L2 caches across SRAM, Si-GCRAM, and Hybrid-GCRAM. Subsequently, we computed the energy consumption ratios of Si-GCRAM and Hybrid-GCRAM, relative to SRAM caches, as presented in Table 6.

These ratios are important metrics in choosing between the three memory technologies under study (SRAM, Si-GCRAM, and Hybrid-GCRAM) and understanding their performance trade-offs for each workload. For instance, specifically for llama-3.2-1b, the higher refresh cost due to the long-lived data in L1 cache makes Si-GCRAM a less energy-efficient option as an L1 cache, compared to SRAM and Hybrid-GCRAM.

On an overall level, the median energy ratio of Si-GCRAM is 0.6213 for the L1 cache and 0.8911 for the L2 cache, while Hybrid-GCRAM exhibit ratios of 0.8481 for the L1 cache and 0.9123 for the L2 cache. Si-GCRAM demonstrates the lowest per-bit read/write energy consumption, making them most energy-efficient for L1 caches where data lifetimes are typically shorter. This efficiency advantage decreases in L2 caches, where longer data lifetimes require more frequent refreshes, leading to higher energy consumption.

Takeaway 7.2. The short-lived data in L1 caches of GPUs favor Si-GCRAM, while L2 caches are better suited for Hybrid-GCRAM due to the longer-lived data they contain.

7.1.4 Write Allocation Policy and Cache Pollution. GainSight’s fine-grained insights into workload behavior and memory-device interactions extend beyond evaluating short-term memories. We demonstrate the profiler’s versatility through a case study on memory allocation policies and cache pollution, as an example of the cross-stack challenges that GainSight can help address.

Cache pollution occurs when data with minimal reuse displaces useful entries [27]. We investigated this by identifying “orphaned accesses” within memory traces—data fetched but never reused

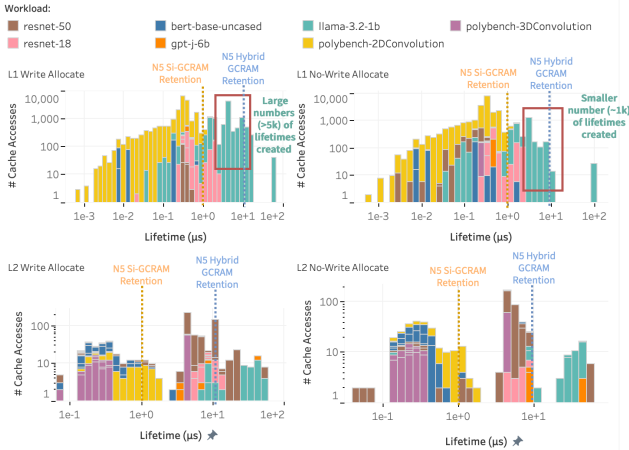


Figure 9: Impact of write allocation policies on data lifetime distribution, compared against simulated 5nm Si-GCRAM and Hybrid-GCRAM retention times [34]. The top and bottom halves show the L1 and L2 caches, respectively; the left and right halves show write-allocate and no-write allocate policies, respectively.

before eviction. We compared the effects of write-allocate versus no-write-allocate policies on data lifetime distributions and orphaned access rates in L1 and L2 caches.

As shown in Figure 9, a no-write-allocate policy significantly reduces short-lived data, especially in L1 caches. This occurs because data written once and read once before eviction are not allocated cache lines under this policy. Eliminating these transient data lifetimes and their associated write operations potentially saves active energy consumption.

Table 7 summarizes the number of orphaned accesses, as a percentage of total read and write accesses to both levels of cache, under both write allocation policies. It can be observed that at least for certain workloads, the number of orphaned accesses is extremely high, particularly in the L1 cache, reaching 97% in bert-base-uncased and gpt-j-6b.

We anticipated that a no-write allocate policy would decrease orphaned accesses by preventing allocation for writes lacking reuse. This expectation held for workloads such as gpt-j-6b, where the policy reduced L1 orphaned accesses from 97% to 48.5%. Conversely,

Table 7: Comparison of orphaned memory accesses between cache levels and write allocation policies

Workload	L1 Orphaned Access %		L2 Orphaned Access %	
	Write Allocate	No Write Allocate	Write Allocate	No Write Allocate
bert-base-uncased	97.06%	95.97%	43.85%	43.25%
gpt-j-6b	97.63%	54.74%	88.28%	48.14%
llama-3.2-1b	80.29%	79.53%	94.74%	93.48%
resnet-18	67.21%	32.27%	50.34%	31.49%
resnet-50	84.32%	42.66%	31.95%	27.47%
polybench-2DConvolution	60.07%	50.97%	56.67%	21.78%
polybench-3DConvolution	48.97%	41.66%	55.89%	38.69%

for bert-base-uncased and llama-3.2-1b, the no-write-allocate policy proved less impactful, primarily due to the workloads’ higher incidence of cache misses on load operations as opposed to stores.

To mitigate inefficiencies arising from cache pollution by orphaned accesses, we advocate for a no-write allocate policy specifically for workloads exhibiting a high proportion of such accesses. Complementary software strategies, including access coalescing or utilizing non-temporal load instructions, could further address orphaned read accesses.

Takeaway 7.3. Up to 97% of cache accesses in a workload may be orphaned. The no-write allocate policy can reduce orphaned accesses significantly (from 97% to 48.5% in some cases), but its effectiveness depends on the workload’s read/write access patterns.

7.2 Profiling Workloads on Systolic Arrays

Systolic arrays have become a predominant hardware architecture adopted by numerous commercial AI/ML accelerators [1, 3, 25, 28, 49]. In our second case study, we extended the open-source cycle-accurate simulator SCALE-Sim [53] for an edge-oriented systolic-array accelerator model, allowing us to investigate data lifetime behaviors in its scratchpad memories. We conducted simulations on three models – ResNet-50 [22], BERT [13], and Llama-3-1B [57] by manually configuring model topology files corresponding to the convolution or GEMM operations in each layer of each model. We note that our focus here is on high-throughput GEMM operations rather than non-linear operations such as normalization, which are not directly mappable to SCALE-Sim and are typically offloaded to dedicated special function units (SFUs) [68, 72]. For BERT and Llama-3-1B, the input sequence length is set to 256 while ResNet-50 receives a 224×224 input image, all with a single batch. We further evaluated these workloads across PE array dimensions of 32x32, 64x64, 128x128, and 256x256 – and across input stationary, weight stationary, and output stationary dataflows. The systolic array accelerator is configured with input, weight, and output buffer capacities of 4kB, 4kB, and 8kB, respectively. The system is set up to have non-restrictive memory bandwidth in order to maximize PE array utilization.

7.2.1 Observations from Lifetime Distributions. Figure 10 presents data lifetime distributions for ResNet-50 executed on a 256 × 256 systolic array under three dataflows: input stationary (*is*), weight stationary (*ws*), and output stationary (*os*). Aggregate calculations reveal that at least 79.01% of data accesses to input, output, and weight buffers are short-lived with lifetimes below 1 μs, suitable for storage in 5nm Si-GCRAM without refresh. Furthermore, the lifetime histograms demonstrate a bimodal distribution with two distinct concentration points: one corresponding to short-duration lifetimes and another to extended-duration lifetimes. The short-duration pattern is attributable to data that is rapidly transferred between on-chip SRAM and either the PE array or main memory. Conversely, extended lifetimes manifest when SRAM buffers experience periods of inactivity following PE array saturation, particularly in configurations where buffer capacity substantially exceeds the computational requirements of the PE array.

7.2.2 Impact of Dataflow on Lifetime. From Figure 10, two key observations stand out. First, short-lived *ofmap* data is present across

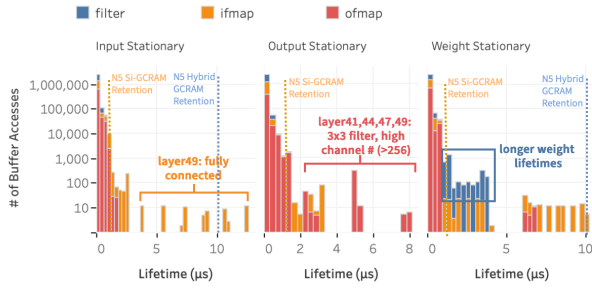


Figure 10: GainSight’s Tableau visualization for a 256×256 systolic array on ResNet-50. Lifetimes are compared against 5nm Si-GCRAM and Hybrid-GCRAM retention times [34].

all dataflows, to the extent that almost all can be stored refresh-free on 5nm Hybrid-GCRAM. This arises from the coupling of PE array timing with output data: the *ofmap* buffer switches when the last output data is written to it. That output data is then written to DRAM, resulting in short *ofmap* lifetimes. This observation on matrix operations in AI workloads having short data lifetimes is consistent with the behavior of GPU kernels discussed in the previous section, presenting an interesting cross-cutting finding. Second, dataflow primarily increases the maximum lifetime of the stationary data, as that data resides longer in its buffer.

Takeaway 7.4. Independent of operation or workload, *ofmap* data exhibits frequent short-lived behavior, while *ifmap* and weight data exhibit a wider distribution of lifetimes with an increased upper-tail when using *is* and *ws* dataflow.

7.2.3 Impact of PE Array Size on Lifetime. Table 8 shows that increasing array size reduces average and maximum lifetimes. Larger arrays result in higher throughput, leading to narrower and more consistent lifetime distributions.

Takeaway 7.5. Scaling up PE array size narrows the lifetime distribution and shifts it towards being shorter-lived, balancing the cost of larger arrays with the potential benefit of integrating more area- and energy-efficient GCRAM.

7.2.4 Observations from Area/Energy Projections. We conducted further analysis on the impact of dataflow configurations on memory buffer area and energy requirements across SRAM, Si-GCRAM and Hybrid-GCRAM. Si-GCRAM and Hybrid-GCRAM take up 41.97% and 22.63% of SRAM’s area, respectively, while consuming 33.23% and 84.81% of SRAM’s energy, respectively, unequivocally pointing to Si-GCRAM as the optimal on-chip memory device for the short-lived data in the scratchpad memories.

These values do not change across dataflows, nor do they change with which on-chip buffer is being considered – across *ifmap*, *filter*, and *ofmap*; this holds true even when the data lifetime distributions across the three dataflows are different. This static relationship may be attributed to the deterministic and fixed dataflow for systolic array buffers. This is in stark contrast to the dynamic behavior of the GPU kernels executing the same workload, when the systolic array does not have to account for non-linear algebra operations such as normalization and pooling.

Table 8: Lifetime Distribution Across PE Array Sizes for ResNet-50 on a 256×256 PE Array

Array Size	<i>ifmap</i>		<i>weight</i>		<i>ofmap</i>	
	Lifetime Avg (ns)	Lifetime Max(ns)	Lifetime Avg (ns)	Lifetime Max(ns)	Lifetime Avg (ns)	Lifetime Max(ns)
32x32	139.1534	68930	123.4484	59219	194.1028	65441
64x64	98.1176	36946	80.0905	12302	188.7503	65441
128x128	63.6960	20850	43.1751	12494	105.7547	16241
256x256	40.4910	12610	28.7488	3650	82.3693	7929

Takeaway 7.6. Si-GCRAM is the most area- and energy-efficient memory device for short-lived data in systolic array accelerators calculating GEMM operations, regardless of dataflow configuration.

8 DISCUSSION

We have presented GainSight, a profiling framework that analyzes memory access patterns and data lifetimes on domain-specific accelerators. The following section summarizes cross-cutting architectural design implications we identified from our experiments, as well as our consideration of how GainSight relates to both short- and long-term memory devices.

8.1 Architectural Implications

GainSight and its case studies demonstrate that runtime profile data can yield meaningful insights and guide design decisions for heterogeneous on-chip memory architectures.

Our experiments consistently indicate a clear distinction between long- and short-lived data across diverse workloads and architectures. Notably, linear algebra operations, while computationally intensive, involve shorter-lived data, making them more compatible with short-term GCRAM, while nonlinear operations which generate longer-lived data may be better suited for long-term GCRAM. Consequently, future AI accelerator architectures should consider heterogeneous on-chip memory solutions, pairing specific kernels with appropriate memory devices: for instance, matrix multiply-accumulate (MAC) units could be paired with short-term on-chip scratchpads, while special function units (SFUs) [26, 48] for normalization, pooling, and softmax could be paired with long-term on-chip caches.

8.2 Future of GCRAM Scaling

In the case of GCRAM devices, prior work [34] highlights scaling challenges: decreasing process nodes increases leakage power and reduces retention time in both Si-GCRAM and Hybrid-GCRAM, even as technologies such as Gate-All-Around (GAA) FETs [69] can reduce the off-current of transistors due to enhanced gate control compared to FinFETs. However, we still believe that GCRAM will continue to be a viable option for short-term on-chip memory arrays. Notably, the expected improvement in operating frequency with smaller process nodes mitigates retention requirements, as more increasing clock frequencies allow for more instructions to be completed within a given time frame, reducing real-world lifetimes. Additionally, various circuit-level techniques are available to further enhance retention times in advanced technology nodes [21, 71].

8.3 GainSight for Other Emerging Memories

Although GainSight’s experimental focus in this work is on short-term GCRAM, the functionalities of the profiler can extend to other long-term non-volatile memory technologies, such as MRAM and RRAM. Its method for analyzing read/write behaviors can be adapted to evaluate these devices, assessing the impact of write latency and endurance on array design. As an example first demonstrated in Section 7.1.4, the issue of cache pollution and low data reuse rates observed in the NVIDIA H100 GPU’s L1/L2 caches implies that incorporating endurance-constrained long-term devices would require strategies such as write coalescing or batching to reduce write frequency and improve data reuse, in order to mitigate the drawbacks of long-term memory devices in write-intensive workloads.

9 CONCLUSION

In summary, GainSight – a profiling framework for memory access patterns and data lifetimes on domain-specific accelerators – is validated through case studies on NVIDIA GPUs and systolic array accelerators. We hope that this open-source tool will inform the design of next-generation AI accelerators, and to help designers make informed decisions about the heterogeneous composition of emerging memory technologies.

REFERENCES

- [1] AMD. 2025. AMD Versal™ AI Edge Series Gen 2. <https://www.amd.com/en/products/adaptive-socs-and-fpgas/versal/gen2/ai-edge-series.html>
- [2] AMD ROCm™ Software. 2025. ROCm/rocprowler. <https://github.com/ROCm/rocprowler> original-date: 2018-07-17T15:49:55Z.
- [3] Arm. 2025. Accelerate Edge AI Innovation. <https://www.arm.com/products/silicon-ip-cpu/ethos/ethos-u85>
- [4] Arghavan Asad, Rupinder Kaur, and Farah Mohammadi. 2022. A Survey on Memory Subsystems for Deep Neural Network Accelerators. *Future Internet* 14, 5 (May 2022), 146. doi:10.3390/fi14050146 Number: 5 Publisher: Multidisciplinary Digital Publishing Institute.
- [5] Cesar Avalos Baddouh, Mahmoud Khairy, Roland N. Green, Mathias Payer, and Timothy G. Rogers. 2021. Principal Kernel Analysis: A Tractable Methodology to Simulate Scaled GPU Workloads. In *MICRO-54: 54th Annual IEEE/ACM International Symposium on Microarchitecture (MICRO '21)*. Association for Computing Machinery, New York, NY, USA, 724–737. doi:10.1145/3466752.3480100
- [6] Ali Bakhoda, George L. Yuan, Wilson W. L. Fung, Henry Wong, and Tor M. Aamodt. 2009. Analyzing CUDA workloads using a detailed GPU simulator. In *2009 IEEE International Symposium on Performance Analysis of Systems and Software*. 163–174. doi:10.1109/ISPASS.2009.4919648
- [7] Andrea Bonetti, Roman Golman, Robert Gitterman, Adam Teman, and Andreas Burg. 2020. Gain-Cell Embedded DRAMs: Modeling and Design Space. *IEEE Transactions on Very Large Scale Integration (VLSI) Systems* 28, 3 (March 2020), 646–659. doi:10.1109/TVLSI.2019.2955933 Conference Name: IEEE Transactions on Very Large Scale Integration (VLSI) Systems.
- [8] Tom B. Brown, Benjamin Mann, Nick Ryder, Melanie Subbiah, Jared Kaplan, Prafulla Dhariwal, Arvind Neelakantan, Pranav Shyam, Girish Sastry, Amanda Askell, Sandhini Agarwal, Ariel Herbert-Voss, Gretchen Krueger, Tom Henighan, Rewon Child, Aditya Ramesh, Daniel M. Ziegler, Jeffrey Wu, Clemens Winter, Christopher Hesse, Mark Chen, Eric Sigler, Mateusz Litwin, Scott Gray, Benjamin Chess, Jack Clark, Christopher Berner, Sam McCandlish, Alec Radford, Ilya Sutskever, and Dario Amodei. 2020. Language Models are Few-Shot Learners. doi:10.48550/arXiv.2005.14165 arXiv:2005.14165 [cs].
- [9] Jian Chen, Koustav Jana, Qi Jiang, Shuhan Liu, Kasidit Toprasertpong, and H.-S. Philip Wong. 2024. (Invited) Oxide Semiconductor Gain Cell Memory. *ECS Meeting Abstracts MA2024-01*, 30 (aug 2024), 1495. doi:10.1149/MA2024-01301495mtgabs
- [10] Xizi Chen, Jingyang Zhu, Jingbo Jiang, and Chi-Ying Tsui. 2019. CompRRAE: RRAM-based convolutional neural network accelerator with reduced computations through a runtime activation estimation. In *Proceedings of the 24th Asia and South Pacific Design Automation Conference (Tokyo, Japan) (ASP-DAC '19)*. Association for Computing Machinery, New York, NY, USA, 133–139. doi:10.1145/3287624.3287640
- [11] Yunji Chen, Tao Luo, Shaoli Liu, Shijin Zhang, Liqiang He, Jia Wang, Ling Li, Tianshi Chen, Zhiwei Xu, Ninghui Sun, and Olivier Temam. 2014. DaDianNao: A Machine-Learning Supercomputer. In *2014 47th Annual IEEE/ACM International Symposium on Microarchitecture*. 609–622. doi:10.1109/MICRO.2014.58 ISSN: 2379-3155.
- [12] Sungsoo Cheon, Kyeongho Lee, and Jongsun Park. 2023. A 2941-TOPS/W Charge-Domain 10T SRAM Compute-in-Memory for Ternary Neural Network. *IEEE Transactions on Circuits and Systems I: Regular Papers* 70, 5 (May 2023), 2085–2097. doi:10.1109/TCSI.2023.3241385
- [13] Jacob Devlin, Ming-Wei Chang, Kenton Lee, and Kristina Toutanova. 2019. BERT: Pre-training of Deep Bidirectional Transformers for Language Understanding. doi:10.48550/arXiv.1810.04805 arXiv:1810.04805 [cs].
- [14] Patrick Esser, Sumith Kulal, Andreas Blattmann, Rahim Entezari, Jonas Müller, Harry Saini, Yam Levi, Dominik Lorenz, Axel Sauer, Frederic Boesel, Dustin Podell, Tim Dockhorn, Zion English, Kyle Lacey, Alex Goodwin, Yannik Marek, and Robin Rombach. 2024. Scaling Rectified Flow Transformers for High-Resolution Image Synthesis. doi:10.48550/arXiv.2403.03206 arXiv:2403.03206 [cs].
- [15] Amir Gholami, Zhewei Yao, Sehoon Kim, Coleman Hooper, Michael W. Mahoney, and Kurt Keutzer. 2024. AI and Memory Wall. *IEEE Micro* 44, 3 (May 2024), 33–39. doi:10.1109/MM.2024.3373763 Conference Name: IEEE Micro.
- [16] Massimo Giordano, Kartik Prabhu, Kalhan Koul, Robert M. Radway, Albert Gural, Rohan Doshi, Zainab F. Khan, John W. Kustin, Timothy Liu, Gregorio B. Lopes, Victor Turbiner, Win-San Khwa, Yu-Der Chih, Meng-Fan Chang, Guénoé Lalleme, Boris Murmann, Subhasish Mitra, and Priyanka Raina. 2021. CHIMERA: A 0.92 TOPS, 2.2 TOPS/W Edge AI Accelerator with 2 MByte On-Chip Foundry Resistive RAM for Efficient Training and Inference. In *2021 Symposium on VLSI Circuits*. 1–2. doi:10.23919/VLSICircuits52068.2021.9492347 ISSN: 2158-5636.
- [17] Robert Gitterman, Amir Shalom, Andreas Burg, Alexander Fish, and Adam Teman. 2020. A 1-Mbit Fully Logic-Compatible 3T Gain-Cell Embedded DRAM in 16-nm FinFET. *IEEE Solid-State Circuits Letters* 3 (2020), 110–113. doi:10.1109/LSSC.2020.3006496 Conference Name: IEEE Solid-State Circuits Letters.
- [18] Aaron Grattafiori, Abhimanyu Dubey, Abhinav Jauhri, Abhinav Pandey, Abhishek Kadian, Ahmad Al-Dahle, Aiesha Letman, Akhil Mathur, Alan Schelten, Alex Vaughan, Amy Yang, Angela Fan, Anirudh Goyal, Anthony Hartshorn, Aobo Yang, Archi Mitra, Archie Sravankumar, Artem Korenev, Arthur Hinsvark, Arun Rao, Aston Zhang, Aurelien Rodriguez, Austen Gregerson, Ava Spataru, Baptiste Roziere, Bethany Biron, Binh Tang, Bobbie Chern, Charlotte Caucheteux, Chaya Nayak, Chloé Bi, Chris Marra, Chris McConerny, Christophe Keller, Christophe Touret, Chunyang Wu, Corinne Wong, Cristian Canton Ferrer, Cyrus Nikolaidis, Damien Allions, Daniel Song, Danielle Pintz, Danny Livshits, Danny Wyatt, David Esiohub, Dhruv Choudhary, Dhruv Mahajan, Diego Garcia-Olano, Diego Perino, Dieuwke Hupkes, Egor Lakomkin, Ehab AlBadawy, Elina Lobanova, Emily Dinan, Eric Michael Smith, Filip Radenovic, Francisco Guzmán, Frank Zhang, Gabriel Synnaeve, Gabrielle Lee, Georgia Lewis Anderson, Govind Thattai, Graeme Nail, Gregoire Mialon, Guan Pang, Guillem Cucurell, Hailey Nguyen, Hannah Koevaar, Hu Xu, Hugo Touvron, Iliyan Zarov, Imanol Arrieta Ibarra, Isabel Kloumann, Ishan Misra, Ivan Evtimov, Jack Zhang, Jade Copet, Jaewon Lee, Jan Geffert, Jana Vranes, Jason Park, Jay Mahadeokar, Jeet Shah, Jelmer van der Linde, Jennifer Billock, Jenny Hong, Jenya Lee, Jeremy Fu, Jianfeng Chi, Jianyu Huang, Jiawen Liu, Jie Wang, Jiecao Yu, Joanna Bitton, Joe Spisak, Jongsoo Park, Joseph Rocca, Joshua Johnstun, Joshua Saxe, Junteng Jia, Kalyan Vasuden Alwala, Karthik Prasad, Kartikeya Upasani, Kate Plawiak, Ke Li, Kenneth Heafield, Kevin Stone, Khalid El-Arini, Krithika Iyer, Kshitiz Malik, Kuenye Chiu, Kunal Bhatta, Kushal Lakhotia, Lauren Rantala-Young, Laurens van der Maaten, Lawrence Chen, Liang Tan, Liz Jenkins, Louis Martin, Lovish Madaan, Lubo Malo, Lukas Blecher, Lukas Landzaat, Luke de Oliveira, Madeline Muzzi, Mahesh Paspuleti, Mannat Singh, Manohar Paluri, Marcin Kardas, Maria Tsimpoukelli, Mathew Oldham, Mathieu Rita, Maya Pavlova, Melanie Kambadur, Mike Lewis, Min Si, Mitesh Kumar Singh, Mona Hassan, Naman Goyal, Narjes Torabi, Nikolay Bashlykov, Nikolay Bogoychev, Niladri Chatterji, Ning Zhang, Olivier Duchenne, Onur Celebi, Patrick Alrassy, Pengchuan Zhang, Pengwei Li, Petar Vasic, Peter Weng, Prajwal Bhargava, Pratik Dubal, Praveen Krishnan, Punit Singh Koura, Puxin Xu, Qing He, Qingxiao Dong, Ragavan Srinivasan, Raj Ganapathy, Ramon Calderer, Ricardo Silveira Cabral, Robert Stojnic, Roberta Raileanu, Rohan Maheswari, Rohit Girdhar, Rohit Patel, Romain Sauvestre, Ronnie Polidoro, Roshan Sumbaly, Ross Taylor, Ruan Silva, Rui Hou, Rui Wang, Saghar Hosseini, Sahana Chennabasappa, Sanjay Singh, Sean Bell, Seohyun Sonia Kim, Sergey Edunov, Shao-liang Nie, Sharan Narang, Sharath Raparthy, Sheng Shen, Shengye Wan, Shruti Bhosale, Shun Zhang, Simon Vandenhende, Soumya Batra, Spencer Whitman, Sten Sootla, Stephane Collet, Suchin Gururangan, Sydney Borodinsky, Tamar Herman, Tara Fowler, Tarek Sheasha, Thomas Georgi, Thomas Scialom, Tobias Speckbacher, Todor Mihaylov, Tong Xiao, Ujjwal Karn, Vedanuj Goswami, Vibhor Gupta, Vignesh Ramanathan, Viktor Kerkez, Vincent Gouget, Virginie Do, Vish Vogeti, Vitor Albiero, Vladan Petrovic, Weiwei Chu, Wenhan Xiong, Wenyan Fu, Whitney Meers, Xavier Martinet, Xiaodong Wang, Xiaofang Wang, Xiaoqing Ellen Tan, Xide Xia, Xinfeng Xie, Xuchao Jia, Xuwei Wang, Yaelle Goldschlag, Yashesh Gaur, Yasmine Babaei, Yi Wen, Yiwen Song, Yuchen

- Zhang, Yue Li, Yuning Mao, Zacharie Delpierre Coudert, Zheng Yan, Zhengxing Chen, Zoe Papakipos, Aaditya Singh, Aayushi Srivastava, Abha Jain, Adam Kelsey, Adam Shajmfeld, Adithya Gangidi, Adolfo Victoria, Ahuva Goldstand, Ajay Menon, Ajay Sharma, Alex Boesenberg, Alexei Baevski, Allie Feinstein, Amanda Kallet, Amit Sangani, Amos Teo, Anam Yunus, Andrei Lupu, Andres Alvarado, Andrew Caples, Andrew Gu, Andrew Ho, Andrew Poulton, Andrew Ryan, Ankit Ramchandani, Annie Dong, Annie Franco, Anuj Goyal, Aparajita Saraf, Arkabandhu Chowdhury, Ashley Gabriel, Ashwin Bharambe, Assaf Eisenman, Azadeh Yazdan, Beau James, Ben Maurer, Benjamin Leonhardt, Bernie Huang, Beth Loyd, Beto De Paola, Bhargavi Paranjape, Bing Liu, Bo Wu, Boyu Ni, Braden Hancock, Bram Wasti, Brandon Spence, Brani Stojkovic, Brian Gamido, Britt Montalvo, Carl Parker, Carly Burton, Catalina Mejia, Ce Liu, Changhan Wang, Changkyu Kim, Chao Zhou, Chester Hu, Ching-Hsiang Chu, Chris Cai, Chris Tindal, Christoph Feichtenhofer, Cynthia Gao, Damon Civin, Dana Beaty, Daniel Kreymer, Daniel Li, David Adkins, David Xu, Davide Testuggine, Delia David, Devi Parikh, Diana Liskovich, Didem Foss, Dingkan Wang, Duc Le, Dustin Holland, Edward Dowling, Eissa Jamil, Elaine Montgomery, Eleonora Prensani, Emily Hahn, Emily Wood, Eric-Tuan Le, Erik Brinkman, Esteban Arcaute, Evan Dunbar, Evan Smothers, Fei Sun, Felix Kreuk, Feng Tian, Filippos Kokkinos, Firat Ozgenel, Francesco Caggioni, Frank Kanayet, Frank Seide, Gabriela Medina Florez, Gabriella Schwarz, Gada Badeer, Georgia Swee, Gil Halpern, Grant Herman, Grigory Sizov, Guangyi Zhang, Guna Lakshminarayanan, Hakan Inan, Hamid Shojanazeri, Han Zou, Hannah Wang, Hanwen Zha, Haroun Habeeb, Harrison Rudolph, Helen Suk, Henry Aspegren, Hunter Goldman, Hongyuan Zhan, Ibrahim Damlaj, Igor Molybog, Igor Tufanov, Ilias Leontiadis, Irina-Elena Veliche, Itai Gat, Jake Weissman, James Geboski, James Kohli, Janice Lam, Japhet Asher, Jean-Baptiste Gaya, Jeff Marcus, Jeff Tang, Jennifer Chan, Jenny Zhen, Jeremy Reizenstein, Jeremy Teboul, Jessica Zhong, Jian Jin, Jingyi Yang, Joe Cummings, Jon Carvill, Jon Shepard, Jonathan McPhie, Jonathan Torres, Josh Ginsburg, Junjie Wang, Kai Wu, Kam Hou U, Karan Saxena, Kartikay Khandelwal, Katayoun Zand, Kathy Matosich, Kaushik Veeraraghavan, Kelly Michelena, Keqian Li, Kiran Jagadeesh, Kun Huang, Kunal Chawla, Kyle Huang, Lailin Chen, Lakshya Garg, Lavender A, Leandro Silva, Lee Bell, Lei Zhang, Liangpeng Guo, Licheng Yu, Liron Moshkovich, Luca Wehrstedt, Madian Khabza, Manav Avalani, Manish Bhatt, Martynas Mankus, Matan Hasson, Matthew Lennie, Matthias Reso, Maxim Groshev, Maxim Naumov, Maya Lathi, Meghan Kenally, Miao Liu, Michael L. Seltzer, Michal Valko, Michelle Restrepo, Mihir Patel, Mik Vyatskov, Mikayel Samvelyan, Mike Clark, Mike Macey, Mike Wang, Miquel Jubert Hermoso, Mo Metanat, Mohammad Rastegari, Munish Bansal, Nandhini Santhanam, Natascha Parks, Natasha White, Navyata Bawa, Nayan Singhal, Nick Egebo, Nicolas Usunier, Nikhil Mehta, Nikolay Pavlovich Laptev, Ning Dong, Norman Cheng, Oleg Chernoguz, Olivia Hart, Omkar Salpekar, Ozlem Kalinli, Parkin Kent, Parth Parekh, Paul Saab, Pavan Balaji, Pedro Rittner, Philip Bontrager, Pierre Roux, Piotr Dollar, Polina Zvyagina, Prashant Ratanandani, Pritish Yuvraj, Qian Liang, Rachad Alao, Rachel Rodriguez, Rafi Ayub, Raghotham Murthy, Raghu Nayani, Rahul Mitra, Rangaprabhu Parthasarathy, Raymond Li, Rebekkah Hogan, Robin Battey, Rocky Wang, Russ Howes, Ruty Rinott, Sachin Mehta, Sachin Siby, Sai Jayesh Bondu, Samyak Datta, Sara Chugh, Sara Hun, Sargun Dhillon, Sasha Sidorov, Satadru Pan, Saurabh Mahajan, Saurabh Verma, Seiji Yamamoto, Sharadh Ramaswamy, Shaun Lindsay, Shaun Lindsay, Sheng Feng, Shenghao Lin, Shengxin Cindy Zha, Shishir Patil, Shiva Shankar, Shuqi Zhang, Shuqiang Zhang, Sinong Wang, Sneha Agarwal, Soji Sajuyigbe, Soumith Chintala, Stephanie Max, Stephen Chen, Steve Kehoe, Steve Satterfield, Sudarshan Govindaprasad, Sumit Gupta, Summer Deng, Sungmin Cho, Sunny Virk, Suraj Subramanian, Sy Choudhury, Sydney Goldman, Tal Remez, Tamar Glaser, Tamara Best, Thilo Koehler, Thomas Robinson, Tianhe Li, Tianjun Zhang, Tim Matthews, Timothy Chou, Tzook Shaked, Varun Vontimitta, Victoria Ajayi, Victoria Montanez, Vijai Mohan, Vinay Satish Kumar, Vishal Mangla, Vlad Ionescu, Vlad Poenaru, Vlad Tiberiu Mihalescu, Vladimir Ivanov, Wei Li, Wenchen Wang, Wenwen Jiang, Wes Bouaziz, Will Constable, Xiaocheng Tang, Xiaojian Wu, Xiaolan Wang, Xilun Wu, Xinbo Gao, Yaniv Kleinman, Yanjun Chen, Ye Hu, Ye Jia, Ye Qi, Yenda Li, Yilin Zhang, Ying Zhang, Yossi Adi, Youngjin Nam, Yu, Wang, Yu Zhao, Yuchen Hao, Yundi Qian, Yunlu Li, Yuzi He, Zach Rait, Zachary DeVito, Zef Rosnbrick, Zhaoduo Wen, Zhenyu Yang, Zhiwei Zhao, and Zhiyu Ma. 2024. The Llama 3 Herd of Models. doi:10.48550/arXiv.2407.21783 arXiv:2407.21783 [cs].
- [19] Scott Grauer-Gray, Lifan Xu, Robert Searles, Sudhee Ayalasomayajula, and John Cavazos. 2012. Auto-tuning a high-level language targeted to GPU codes. In *2012 Innovative Parallel Computing (InPar)*. 1–10. doi:10.1109/InPar.2012.6339595
- [20] Robert Greenway, Kwangok Jeong, Andrew Kahng, Chul-Hong Park, and John Petersen. 2008. 32nm 1-D Regular Pitch SRAM Bitcell Design for Interference-Assisted Lithography. *Proceedings of SPIE - The International Society for Optical Engineering* 7122 (10 2008). doi:10.1117/12.801883
- [21] Odem Harel, Andac Yigit, Eliana Feifel, Robert Giterman, Andreas Burg, and Adam Teman. 2024. A 16-kB 65-nm GC-eDRAM Macro With Internal Bias Voltage Generation Providing Over 100 μ s Retention Time. *IEEE Journal of Solid-State Circuits* (2024), 1–10. doi:10.1109/JSSC.2024.3489793
- [22] Kaiming He, Xiangyu Zhang, Shaoqing Ren, and Jian Sun. 2015. Deep Residual Learning for Image Recognition. doi:10.48550/arXiv.1512.03385 arXiv:1512.03385 [cs].
- [23] Sepp Hochreiter and Jürgen Schmidhuber. 1997. Long Short-Term Memory. *Neural Computation* 9, 8 (Nov. 1997), 1735–1780. doi:10.1162/neco.1997.9.8.1735 Conference Name: Neural Computation.
- [24] Shao-Chun Hung, Arjun Chaudhuri, Sanmitra Banerjee, and Krishnendu Chakrabarty. 2024. Fault Diagnosis for Resistive Random Access Memory and Monolithic Inter-Tier Vias in Monolithic 3-D Integration. *IEEE Transactions on Very Large Scale Integration (VLSI) Systems* PP (07 2024), 1–14. doi:10.1109/TVLSI.2024.3380549
- [25] Intel. 2025. Intel® NPU Acceleration Library. <https://github.com/intel/intel-npu-acceleration-library>
- [26] Daphne Ippolito, Florian Tramer, Milad Nasr, Chiuyuan Zhang, Matthew Jagielski, Katherine Lee, Christopher Choquette Choo, and Nicholas Carlini. 2023. Preventing Generation of Verbatim Memorization in Language Models Gives a False Sense of Privacy. In *Proceedings of the 16th International Natural Language Generation Conference*, C. Maria Keet, Hung-Yi Lee, and Sina Zarrieß (Eds.), Association for Computational Linguistics, Prague, Czechia, 28–53. doi:10.18653/v1/2023.inlg-main.3
- [27] Prabhat Jain, Srinu Devadas, and Larry Rudolph. 2001. *Controlling Cache Pollution in Prefetching With Software-assisted Cache Replacement*. Memorandum 462. MIT Computer Science and Artificial Intelligence Laboratory, Cambridge, MA. <https://csail.mit.edu/pubs/memos/Memo-462/memo-462.pdf>
- [28] Norman P. Jouppi, Cliff Young, Nishant Patil, David Patterson, Gaurav Agrawal, Raminder Bajwa, Sarah Bates, Suresh Bhatia, Nan Boden, Al Borchers, Rick Boyle, Pierre-luc Cantin, Clifford Chao, Chris Clark, Jeremy Coriell, Mike Daley, Matt Dau, Jeffrey Dean, Ben Gelb, Tara Vazir Ghaemmaghami, Rajendra Gottipati, William Gulland, Robert Hagmann, C. Richard Ho, Doug Hogberg, John Hu, Robert Hundt, Dan Hurt, Julian Ibarz, Aaron Jaffey, Alek Jaworski, Alexander Kaplan, Harshit Khaitan, Daniel Killebrew, Andy Koch, Naveen Kumar, Steve Lacy, James Laudon, James Law, Diemthun Le, Chris Leary, Zhuyuan Liu, Kyle Lucke, Alan Lunn, Gordon MacKean, Adriana Maggiore, Maire Mahony, Kieran Miller, Rahul Nagarajan, Ravi Narayanaswami, Ray Ni, Kathy Nix, Thomas Norrie, Mark Omernick, Narayana Penukonda, Andy Phelps, Jonathan Ross, Matt Ross, Amir Salek, Emad Samadiani, Chris Severn, Gregory Sizikov, Matthew Snellman, Jed Soutter, Dan Steinberg, Andy Swing, Mercedes Tan, Gregory Thorson, Bo Tian, Horia Toma, Erick Tuttle, Vijay Vasudevan, Richard Walter, Walter Wang, Eric Wilcox, and Doe Hyun Yoon. 2017. In-Datacenter Performance Analysis of a Tensor Processing Unit. *SIGARCH Comput. Archit. News* 45, 2 (June 2017), 1–12. doi:10.1145/3140659.3080246
- [29] Mahmoud Khairy, Zhesheng Shen, Tor M. Aamodt, and Timothy G. Rogers. 2020. Accel-Sim: An Extensible Simulation Framework for Validated GPU Modeling. In *2020 ACM/IEEE 47th Annual International Symposium on Computer Architecture (ISCA)*. 473–486. doi:10.1109/ISCA45697.2020.00047
- [30] Sergey Legtchenko, Ioan Stefanovici, Richard Black, Antony Rowstron, Junyi Liu, Paolo Costa, Burcu Canakci, Dushyanth Narayanan, and Xingbo Wu. 2025. Managed-Retention Memory: A New Class of Memory for the AI Era. doi:10.48550/arXiv.2501.09605 arXiv:2501.09605 [cs].
- [31] Ziyun Li, Zhehong Wang, Li Xu, Qing Dong, Bowen Liu, Chin-I Su, Wen-Ting Chu, George Tsou, Yu-Der Chih, Tsung-Yung Jonathan Chang, Dennis Sylvester, Hun-Seok Kim, and David Blaauw. 2021. RRAM-DNN: An RRAM and Model-Compression Empowered All-Weights-On-Chip DNN Accelerator. *IEEE Journal of Solid-State Circuits* 56, 4 (2021), 1105–1115. doi:10.1109/JSSC.2020.3045369
- [32] Linux Foundation. [n. d.]. *perf: Linux Performance Analysis Tools*. <https://man7.org/linux/man-pages/man1/perf.1.html> Accessed: 2025-03-13.
- [33] Hai-Kun Liu, Di Chen, Hai Jin, Xiao-Fei Liao, Binsheng He, Kan Hu, and Yu Zhang. 2021. A survey of non-volatile main memory technologies: State-of-the-arts, practices, and future directions. *Journal of Computer Science and Technology* 36 (2021), 4–32.
- [34] Shuhan Liu, Koustav Jana, Kasidit Toprasertpong, Jian Chen, Zheng Liang, Qi Jiang, Sumaiya Wahid, Shengjun Qin, Wei-Chen Chen, Eric Pop, and H.-S. Philip Wong. 2024. Design Guidelines for Oxide Semiconductor Gain Cell Memory on a Logic Platform. *IEEE Transactions on Electron Devices* 71, 5 (May 2024), 3329–3335. doi:10.1109/TED.2024.3372938 Conference Name: IEEE Transactions on Electron Devices.
- [35] Shuhan Liu, Koustav Jana, Kasidit Toprasertpong, Jian Chen, Zheng Liang, Qi Jiang, Sumaiya Wahid, Shengjun Qin, Wei-Chen Chen, and H.-S. Philip Wong. 2023. Gain Cell Memory on Logic Platform – Device Guidelines for Oxide Semiconductor Transistor Materials Development. In *2023 International Electron Devices Meeting (IEDM)*. 1–4. doi:10.1109/IEDM45741.2023.10413726 ISSN: 2156-017X.
- [36] Shuhan Liu, Shengjun Qin, Koustav Jana, Jian Chen, Kasidit Toprasertpong, and H.-S. Philip Wong. 2024. First Experimental Demonstration of Hybrid Gain Cell Memory with Si PMOS and ITO FET for High-speed On-chip Memory. *2024 IEEE Symposium on VLSI Technology and Circuits (VLSI Technology and Circuits)* (2024), 1–2. <https://api.semanticscholar.org/CorpusID:27197272>

- [37] Margaret Martonosi, Anoop Gupta, and Thomas Anderson. 1992. MemSpy: analyzing memory system bottlenecks in programs. *SIGMETRICS Perform. Eval. Rev.* 20, 1 (June 1992), 1–12. doi:10.1145/149439.133079
- [38] Kaniz Mishy and Mehdi Sadi. 2021. Designing Efficient and High-performance AI Accelerators with Customized STT-MRAM. doi:10.48550/arXiv.2104.02199 arXiv:2104.02199 [cs].
- [39] M. Mukai, Y. Hayashi, and Y. Komatsu. 1999. Proposal of a logic compatible merged-type gain cell for high-density embedded DRAM's. *IEEE Transactions on Electron Devices* 46, 6 (June 1999), 1201–1206. doi:10.1109/16.766885
- [40] Nicholas Nethercote. 2004. *Dynamic binary analysis and instrumentation*. Technical Report UCAM-CL-TR-606. University of Cambridge, Computer Laboratory. doi:10.48456/tr-606
- [41] Duy-Thanh Nguyen, Abhiroop Bhattacharjee, Abhishek Moitra, and Priyadarshini Panda. 2024. MCAIMem: A Mixed SRAM and eDRAM Cell for Area and Energy-Efficient On-Chip AI Memory. *IEEE Transactions on Very Large Scale Integration (VLSI) Systems* 32, 11 (2024), 2023–2036. doi:10.1109/TVLSI.2024.3439231
- [42] NVIDIA Corporation. 2024. Nsight Compute Documentation – NsightCompute 12.6 documentation. <https://docs.nvidia.com/nsight-compute/index.html>
- [43] NVIDIA Corporation. 2025. CUPTI – Cupti 12.8 documentation. <https://docs.nvidia.com/cupti/>
- [44] The pandas development team. 2020. *pandas-dev/pandas: Pandas*. doi:10.5281/zenodo.3509134
- [45] Lillian Pentecost, Alexander Hankin, Marco Donato, Mark Hempstead, Gu-Yeon Wei, and David Brooks. 2022. NVMEExplorer: A Framework for Cross-Stack Comparisons of Embedded Non-Volatile Memories. In *2022 IEEE International Symposium on High-Performance Computer Architecture (HPCA)*, 938–956. doi:10.1109/HPCA53966.2022.00073
- [46] Aleksey Pesterev, Nickolai Zeldovich, and Robert T. Morris. 2010. Locating cache performance bottlenecks using data profiling. In *Proceedings of the 5th European conference on Computer systems (EuroSys '10)*. Association for Computing Machinery, New York, NY, USA, 335–348. doi:10.1145/1755913.1755947
- [47] Louis-Noel Pouchet, Peng Zhang, P. Sadayappan, and Jason Cong. 2013. Polyhedral-based data reuse optimization for configurable computing. In *Proceedings of the ACM/SIGDA international symposium on Field programmable gate arrays (FPGA '13)*. Association for Computing Machinery, New York, NY, USA, 29–38. doi:10.1145/2435264.2435273
- [48] Jiajun Qin, Tianhua Xia, Cheng Tan, Jeff Zhang, and Sai Qian Zhang. 2025. PICACHU: Plug-In CGRA Handling Upcoming Nonlinear Operations in LLMs. In *Proceedings of the 30th ACM International Conference on Architectural Support for Programming Languages and Operating Systems, Volume 2 (ASPLOS '25)*. Association for Computing Machinery, New York, NY, USA, 845–861. doi:10.1145/3676641.3716013
- [49] Qualcomm. 2025. Qualcomm Hexagon NPU. <https://www.qualcomm.com/products/technology/processors/hexagon>
- [50] Vijay Janapa Reddi, Christine Cheng, David Kanter, Peter Mattson, Guenther Schmuelling, Carole-Jean Wu, Brian Anderson, Maximilien Breughe, Mark Charlebois, William Chou, Ramesh Chukka, Cody Coleman, Sam Davis, Pan Deng, Greg Diamos, Jared Duke, Dave Fick, J. Scott Gardner, Itay Hubara, Sachin Iduunji, Thomas B. Jablin, Jeff Jiao, Tom St John, Pankaj Kanwar, David Lee, Jeffery Liao, Anton Lokhmotov, Francisco Massa, Peng Meng, Paulius Mickevicius, Colin Osborne, Gennady Pekhimenko, Arun Tejusve Raghunath Rajan, Dilip Sequeira, Ashish Sirasao, Fei Sun, Hanlin Tang, Michael Thomson, Frank Wei, Ephrem Wu, Lingjie Xu, Koichi Yamada, Bing Yu, George Yuan, Aaron Zhong, Peizhao Zhang, and Yuchen Zhou. 2020. MLPerf Inference Benchmark. doi:10.48550/arXiv.1911.02549 arXiv:1911.02549 [cs].
- [51] Francesco Restuccia and Alessandro Biondi. 2021. Time-Predictable Acceleration of Deep Neural Networks on FPGA SoC Platforms. In *2021 IEEE Real-Time Systems Symposium (RTSS)*. IEEE, Dortmund, DE, 441–454. doi:10.1109/RTSS52674.2021.00047
- [52] Salesforce, Inc. 2025. Tableau Public. <https://www.tableau.com/community/public>
- [53] Ananda Samajdar, Jan Moritz Joseph, Yuhao Zhu, Paul Whatmough, Matthew Mattina, and Tushar Krishna. 2020. A systematic methodology for characterizing scalability of DNN accelerators using SCALE-sim. In *2020 IEEE International Symposium on Performance Analysis of Systems and Software (ISPASS)*. IEEE, 58–68.
- [54] Julian Seward and Nicholas Nethercote. 2002. *Valgrind: Cachegrind – a Cache and Branch-Prediction Profiler*. <https://valgrind.org/docs/manual/cg-manual.html> Accessed: 2025-03-13.
- [55] Taejoong Song, Woojin Rim, Sunghyun Park, Yongho Kim, Giyong Yang, Hoonki Kim, Sanghoon Baek, Jonghoon Jung, Bongjae Kwon, Sungwee Cho, Hyuntaek Jung, Yongjae Choo, and Jaeseung Choi. 2017. A 10 nm FinFET 128 Mb SRAM With Assist Adjustment System for Power, Performance, and Area Optimization. *IEEE Journal of Solid-State Circuits* 52, 1 (Jan. 2017), 240–249. doi:10.1109/JSSC.2016.2609386
- [56] Kasidit Toprasertpong, Shuhan Liu, Jian Chen, Sumaiya Wahid, Koustav Jana, Wei-Chen Chen, Shengman Li, Eric Pop, and H.-S. Philip Wong. 2023. Co-designed Capacitive Coupling-Immune Sensing Scheme for Indium-Tin-Oxide (ITO) 2T Gain Cell Operating at Positive Voltage Below 2 V. (2023), 1–2. doi:10.23919/VLSITechnologyandCir57934.2023.10185433
- [57] Hugo Touvron, Thibaut Lavril, Gautier Izacard, Xavier Martinet, Marie-Anne Lachaux, Timothée Lacroix, Baptiste Rozière, Naman Goyal, Eric Hambro, Faisal Azhar, Aurelien Rodriguez, Armand Joulin, Edouard Grave, and Guillaume Lample. 2023. LLaMA: Open and Efficient Foundation Language Models. doi:10.48550/arXiv.2302.13971 arXiv:2302.13971 [cs].
- [58] Fengbin Tu, Weiwei Wu, Shouyi Yin, Leibo Liu, and Shaojun Wei. 2018. RANA: Towards Efficient Neural Acceleration with Refresh-Optimized Embedded DRAM. In *2018 ACM/IEEE 45th Annual International Symposium on Computer Architecture (ISCA)*, 340–352. doi:10.1109/ISCA.2018.00037 ISSN: 2575-713X.
- [59] Ashish Vaswani, Noam Shazeer, Niki Parmar, Jakob Uszkoreit, Llion Jones, Aidan N Gomez, Łukasz Kaiser, and Illia Polosukhin. 2017. Attention is All you Need. In *Advances in Neural Information Processing Systems*, Vol. 30. Curran Associates, Inc. https://proceedings.neurips.cc/paper_files/paper/2017/hash/3f5ee243547dee91fbd053c1c4a845aa-Abstract.html
- [60] Oreste Villa, Daniel Lustig, Zi Yan, Evgeny Bolotin, Yaosheng Fu, Niladrish Chatterjee, Nan Jiang, and David Nellans. 2021. Need for Speed: Experiences Building a Trustworthy System-Level GPU Simulator. In *2021 IEEE International Symposium on High-Performance Computer Architecture (HPCA)*, 868–880. doi:10.1109/HPCA51647.2021.00077 ISSN: 2378-203X.
- [61] Oreste Villa, Mark Stephenson, David Nellans, and Stephen W. Keckler. 2019. NVBit: A Dynamic Binary Instrumentation Framework for NVIDIA GPUs. In *Proceedings of the 52nd Annual IEEE/ACM International Symposium on Microarchitecture (MICRO '52)*. Association for Computing Machinery, New York, NY, USA, 372–383. doi:10.1145/3352460.3358307
- [62] Ben Wang. 2021. Mesh-Transformer-JAX: Model-Parallel Implementation of Transformer Language Model with JAX. <https://github.com/kingoflolz/mesh-transformer-jax>.
- [63] Ben Wang and Aran Komatsuzaki. 2021. GPT-J-6B: A 6 Billion Parameter Autoregressive Language Model. <https://github.com/kingoflolz/mesh-transformer-jax>.
- [64] Qiwen Wang, Xinxin Wang, Seung Hwan Lee, Fan-Hsuan Meng, and Wei D. Lu. 2019. A Deep Neural Network Accelerator Based on Tiled RRAM Architecture. In *2019 IEEE International Electron Devices Meeting (IEDM)*, 14.4.1–14.4.4. doi:10.1109/IEDM19573.2019.8993641
- [65] Wes McKinney. 2010. Data Structures for Statistical Computing in Python. *Proceedings of the 9th Python in Science Conference*, Stéfan van der Walt and Jarrod Millman (Eds.), 56 – 61. doi:10.25080/Majora-92bf1922-00a
- [66] Tongda Wu, Luchang Lei, Yifan He, Wenbin Jia, Songming Yu, Yuxuan Huang, Hongyang Jia, Huazhong Yang, and Yongpan Liu. 2024. A Heterogeneous Microprocessor for Intermittent AI Inference Using Nonvolatile-SRAM-Based Compute-In-Memory. *IEEE Transactions on Circuits and Systems II: Express Briefs* 71, 11 (Nov. 2024), 4753–4757. doi:10.1109/TCSII.2023.3289493
- [67] Fu-Liang Yang, Cheng-Chuan Huang, Chien-Chao Huang, Tang-Xuan Chung, Hou-Yu Chen, Chang-Yun Chang, Hung-Wei Chen, Di-Hong Lee, Sheng-Da Liu, Kuang-Hsin Chen, Cheng-Kuo Wen, Shui-Ming Cheng, Chang-Ta Yang, Li-Wei Kung, Chiu-Lien Lee, Yu-Jun Chou, Fu-Jye Liang, Lin-Hung Shiu, Jan-Wen You, King-Chang Shu, Bin-Chang Chang, Jaw-Jung Shin, Chun-Kuang Chen, Tsai-Sheng Gau, Ping-Wei Wang, Bor-Wen Chan, Peng-Fu Hsu, Jyu-Hong Shieh, S.K.-H. Fung, C.H. Diaz, C.-M.M. Wu, Yee-Chaung See, B.J. Lin, M.-S. Liang, J.Y.-C. Sun, and Chenming Hu. 2004. 45nm node planar-SOI technology with 0.296 $\mu\text{m}^2/\text{m}^2$ 6T-SRAM cell. In *Digest of Technical Papers. 2004 Symposium on VLSI Technology*, 2004, 8–9. doi:10.1109/VLSIT.2004.1345362
- [68] Jianchao Yang, Mei Wen, Junzhong Shen, Yasong Cao, Minjin Tang, Renyu Yang, Jiawei Fei, and Chunyuan Zhang. 2022. BP-Im2col: Implicit Im2col Supporting AI Backpropagation on Systolic Arrays. arXiv:2209.09434 [cs.AR] <https://arxiv.org/abs/2209.09434>
- [69] Geoffrey Yeap, S.S. Lin, H.L. Shang, H.C. Lin, Y.C. Peng, M. Wang, PW Wang, CP Lin, KF Yu, WY Lee, HK Chen, DW Lin, BR Yang, CC Yeh, CT Chan, JM Kuo, C-M Liu, TH Chiu, MC Wen, TL Lee, CY Chang, R Chen, P-H Huang, C.S. Hou, YK Lin, FK Yang, J. Wang, S. Fung, Ryan Chen, C.H. Lee, TL Lee, W. Chang, DY Lee, CY Ting, T. Chang, HC Huang, HJ Lin, C. Tseng, CW Chang, KB Huang, YC Lu, C-H Chen, C.O. Chui, KW Chen, MH Tsai, CC Chen, N. Wu, HT Chiang, XM Chen, SH Sun, JT Tzeng, K. Wang, YC Peng, HJ Liao, T. Chen, YK Cheng, J. Chang, K. Hsieh, A. Cheng, G. Liu, A. Chen, HT Lin, KC Chiang, CW Tsai, H. Wang, W. Sheu, J. Yeh, YM Chen, CK Lin, J. Wu, M. Cao, LS Juang, F. Lai, Y. Ku, S.M. Jang, and L.C. Lu. 2024. 2nm Platform Technology Featuring Energy-Efficient Nanosheet Transistors and Interconnects Co-Optimized with 3DIC for AI, HPC and Mobile SoC Applications. In *2024 IEEE International Electron Devices Meeting (IEDM)*, 1–4. doi:10.1109/IEDM50854.2024.10873475 ISSN: 2156-017X.
- [70] Geoffrey Yeap, S. S. Lin, Y. M. Chen, H. L. Shang, P. W. Wang, H. C. Lin, Y. C. Peng, J. Y. Sheu, M. Wang, X. Chen, B. R. Yang, C. P. Lin, F. C. Yang, Y. K. Leung, D. W. Lin, C. P. Chen, K. F. Yu, D. H. Chen, C. Y. Chang, H. K. Chen, P. Hung, C. S. Hou, Y. K. Cheng, J. Chang, L. Yuan, C. K. Lin, C. C. Chen, Y. C. Yeo, M. H. Tsai, H. T. Lin, C. O. Chui, K. B. Huang, W. Chang, H. J. Lin, K. W. Chen, R. Chen,

- S. H. Sun, Q. Fu, H. T. Yang, H. T. Chiang, C. C. Yeh, T. L. Lee, C. H. Wang, S. L. Shue, C. W. Wu, R. Lu, W. R. Lin, J. Wu, F. Lai, Y. H. Wu, B. Z. Tien, Y. C. Huang, L. C. Lu, Jun He, Y. Ku, J. Lin, M. Cao, T. S. Chang, and S. M. Jang. 2019. 5nm CMOS Production Technology Platform featuring full-fledged EUV, and High Mobility Channel FinFETs with densest $0.021\mu\text{m}^2$ SRAM cells for Mobile SoC and High Performance Computing Applications. In *2019 IEEE International Electron Devices Meeting (IEDM)*. 36.7.1–36.7.4. doi:10.1109/IEDM19573.2019.8993577 ISSN: 2156-017X.
- [71] Andac Yigit, Emmanuel Nieto Casarrubias, Robert Giterman, and Andreas Burg. 2023. A 128-kbit GC-eDRAM With Negative Boosted Bootstrap Driver for 11.3x Lower-Refresh Frequency at a 2.5% Area Overhead in 28-nm FD-SOI. *IEEE Solid-State Circuits Letters* 6 (2023), 13–16. doi:10.1109/LSSC.2022.3232775
- [72] Sai Qian Zhang, Thierry Tambe, Nestor Cuevas, Gu-Yeon Wei, and David Brooks. 2024. CAMEL: Co-Designing AI Models and eDRAMs for Efficient On-Device Learning. In *2024 IEEE International Symposium on High-Performance Computer Architecture (HPCA)*. 861–875. doi:10.1109/HPCA57654.2024.00071 ISSN: 2378-203X.
- [73] Mai Zheng, Vignesh T. Ravi, Wenjing Ma, Feng Qin, and Gagan Agrawal. 2012. GMProf: A low-overhead, fine-grained profiling approach for GPU programs. In *2012 19th International Conference on High Performance Computing*. 1–10. doi:10.1109/HiPC.2012.6507475